# SIMULATION OF WIND FIELDS OVER POINT ARGUELLO, CALIFORNIA, BY WIND-TUNNEL FLOW OVER A TOPOGRAPHIC MODEL

by

J. E. Cermak and Jon Peterka



November 1966

CER65JEC-JAP64

# SIMULATION OF WIND FIELDS OVER POINT ARGUELLO, CALIFORNIA, BY WIND-TUNNEL FLOW OVER A TOPOGRAPHIC MODEL

by

J. E. Cermak and Jon Peterka

Prepared under
U. S. Navy Contract N123(61756)34361A(PMR)
U. S. Navy Purchasing Office
Los Angeles, California

Fluid Dynamics and Diffusion Laboratory
College of Engineering
Colorado State University
Fort Collins, Colorado

November 1966

CER65JEC-JAP64

## ABSTRACT

Stably stratified flow over a 1:12,000 scale model of the U. S. Naval Missile Facility at Point Arguello, California was studied in the Army Meteorological wind tunnel of the Fluid Dynamics and Diffusion Laboratory at Colorado State University. Mean temperature, mean velocity and mean concentration distributions obtained for the laboratory flow were compared with available field data collected at the site. These comparisons revealed that the geometrical, dynamic and thermal similarity were sufficiently achieved to give similar mean flow patterns, temperature distributions and concentration decay rates for diffusing tracers.

The data revealed that a laminar laboratory flow may be used to simulate a turbulent field flow under conditions of stable thermal stratification and complex terrain. In such flow conditions, diffusion is dominated by convective dispersion.

## ACKNOWLEDGMENTS

Many individuals working in the Fluid Mechanics Program at Colorado State University have made major contributions to this study. The assistance of Mr. Jiri Myska has added materially to the completion of this effort.

TABLE OF CONTENTS


| Chapter | | Page |
|---|---|---|
| | LIST OF FIGURES | v |
| | LIST OF SYMBOLS | viii |
| I. | INTRODUCTION | 1 |
| II. | EXPERIMENTAL EQUIPMENT | 3 |
| | A. Wind Tunnel | 3 |
| | B. Instrumentation | 3 |
| | C. Models | 5 |
| III. | FLOW SIMILARITY | 6 |
| | A. Geometrical Similarity | 6 |
| | B. Reynolds-Number Similarity | 6 |
| | C. Thermal Similarity | 10 |
| IV. | CHARACTERISTICS OF THE MODEL FLOW AND COMPARISON WITH THE PROTOTYPE FLOW | 13 |
| | A. Boundary-Layer Characteristics Upwind From the Model | 13 |
| | B. Temperature and Velocity Fields Over the Model | 15 |
| | C. Flow Patterns Over the Model | 18 |
| | D. Diffusion Measurements | 21 |
| V. | CONCLUSIONS | 24 |
| | BIBLIOGRAPHY | 25 |
| | FIGURES | 26 |

LIST OF FIGURES


| Figure | | Page |
|---|---|---|
| 1 | Topographic map of the model of Point Arguello, California | 26 |
| 2 | Distribution of Richardson numbers for Point Arguello, California | 27 |
| 3 | Bulk Richardson number for boundary-layer flow | 28 |
| 4 | Typical approach-flow velocity profiles | 29 |
| 5 | Typical approach-flow temperature profiles | 30 |
| 6 | Model of Point Arguello showing data cross section lines | 31 |
| 7 | Vertical cross section showing constant-temperature lines | 32 |
| 8 | Vertical cross section showing constant-temperature lines | 33 |
| 9 | Vertical cross section showing constant-velocity lines | 34 |
| 10 | Vertical cross section showing constant-velocity lines | 35 |
| 11 | Temperature variations at constant elevations | 36 |
| 12 | Velocity variations at constant elevations | 37 |
| 13 | Non-dimensional temperature profiles for field data at data point No. 16 | 38 |
| 14 | Non-dimensional temperature profiles for field data at data point No. 1 | 39 |
| 15 | Non-dimensional temperature profiles for wind-tunnel data at data points Nos. 1, 6, 10, 16 | 40 |

LIST OF FIGURES - continued


| Figure | | Page |
|---|---|---|
| 16 | Non-dimensional temperature profiles for field data at data points Nos. 1, 6, 10, 16 . . . . . | 41 |
| 17 | Single release ammonia-trace data . . . . . | 42 |
| 18 | Multiple release ammonia-trace data . . . . . | 43 |
| 19 | Smoke-flow patterns for 340° ambient flow direction . . | 44 |
| 20 | Smoke-flow patterns for 340° ambient flow direction . . | 45 |
| 21 | Smoke-flow patterns for 340° ambient flow direction . . | 46 |
| 22 | Smoke-flow patterns for 340° ambient flow direction . . | 47 |
| 23 | Smoke-flow patterns for 340° ambient flow direction . . | 48 |
| 24 | Smoke-flow patterns for 340° ambient flow direction . . | 49 |
| 25 | Smoke-flow patterns for 340° ambient flow direction . . | 50 |
| 26 | Smoke-flow patterns for 340° ambient flow direction . . | 51 |
| 27 | Smoke-flow patterns for 315° ambient flow direction . . | 52 |
| 28 | Smoke-flow patterns for 315° ambient flow direction . . | 53 |
| 29 | Smoke-flow patterns for 315° ambient flow direction . . | 54 |
| 30 | Smoke-flow patterns for 315° ambient flow direction . . | 55 |
| 31 | Smoke-flow patterns for 315° ambient flow direction . . | 56 |
| 32 | Smoke-flow patterns for 315° ambient flow direction . . | 57 |
| 33 | Smoke-flow patterns for 315° ambient flow direction . . | 58 |
| 34 | Smoke-flow patterns for 315° ambient flow direction . . | 59 |
| 35 | Smoke-flow patterns for 315° ambient flow direction . . | 60 |

LIST OF FIGURES - continued


| Figure | | Page |
|---|---|---|
| 36 | Smoke-flow patterns for 315° ambient flow direction . . | 61 |
| 37 | Smoke-flow patterns for 315° ambient flow direction . . | 62 |
| 38 | Mean-flow patterns for 340° ambient flow direction with inversion conditions . . . . . | 63 |
| 39 | Mean-flow patterns for 315° ambient flow direction with inversion conditions . . . . . | 64 |
| 40 | Mean-flow patterns for 315° ambient flow direction with neutral conditions . . . . . | 65 |
| 41 | Comparison of wind-tunnel and prototype flow patterns for inversion flow with 340° ambient wind direction . . . | 66 |
| 42 | Comparison of wind tunnel and prototype flow patterns for inversion flow with 315° ambient wind direction . . . | 67 |
| 43 | Comparison of diffusion trajectories for source in Hondo Canyon -- 340° wind . . . . . | 68 |
| 44 | Distribution of ground-level sampling points . . . . . | 69 |
| 45 | Ground-level concentration distributions normal to plume axis . . . . . | 70 |
| 46 | Ground-level concentration distributions normal to plume axis . . . . . | 71 |
| 47 | Ground-level concentration distributions normal to plume axis . . . . . | 72 |
| 48 | Ground-level concentration distributions normal to plume axis . . . . . | 73 |
| 49 | Ground-level concentration distributions normal to plume axis . . . . . | 74 |
| 50 | Downwind variation of dilution and concentration . . . . | 75 |

## LIST OF SYMBOLS

| Symbols | | Dimensions |
|---|---|---|
| $c$ | Instantaneous concentration fluctuation from mean | ppm |
| $\overline{C}$ | Time mean concentration | ppm |
| $g$ | Acceleration of gravity | $ft/sec^2$ |
| $h$ | Typical roughness height | ft |
| $i$ | Subscript to indicate ith coordinate | |
| $H$ | Height of a characteristic feature | ft |
| $K_H$ | Exchange coefficient for heat | $lb_f\text{-}sec/ft^2$ |
| $K_M$ | Exchange coefficient for momentum | $lb_f\text{-}sec/ft^2$ |
| $R$ | Reynolds number | |
| $R_f$ | Richardson number in the flux form | |
| $Ri$ | Richardson number | |
| $Ri(Crit.)$ | Critical Richardson number | |
| $t$ | Time | sec |
| $T_a$ | Potential temperature at elevation z | $^0R$ |
| $T_w$ | Potential temperature at the surface | $^0R$ |
| $T_\infty$ | Potential temperature of the ambient flow | $^0R$ |
| $u$ | Local mean velocity | ft/sec |
| $U$ | Ambient velocity | ft/sec |

LIST OF SYMBOLS - continued

| Symbols | | Dimensions |
|---|---|---|
| $x$ | Cartesian coordinate | ft |
| $z$ | Elevation | ft |
| $\delta$ | Boundary-layer thickness | ft |
| $\eta$ | Coefficient of mass diffusion | $ft^2/sec$ |
| $\theta$ | Potential temperature | $^0R$ |
| $\nu$ | Kinematic viscosity | $ft^2/sec$ |

# I. INTRODUCTION

A wind-tunnel study of Point Arguello was motivated by the desire to estimate the diffusion characteristics of toxic gases which might be released in the vicinity of missile launch sites on the U. S. Naval Missile Facility. A necessary condition for the modeling of diffusion characteristics is that mean flow patterns over a scale model of the terrain be established which are similar to those in the prototype. Accordingly, the primary purpose of this study was to determine if wind patterns observed in a wind tunnel over a 1:12,000 scale model of the Point Arguello area are representative of actual wind patterns observed in the field. During this study, conducted in the Army Meteorological Wind Tunnel of the Colorado State University Fluid Dynamics and Diffusion Laboratory, emphasis was placed on stably stratified flows. This emphasis was required by the fact that the prototype flows are usually stably stratified.

The study was exploratory in nature since no attempt had been made in previous studies to model wind patterns with thermal stratification using such a small scale model with the exception of a 1:50,000 model study of the lee-wave formation downwind of Mt. Fuji by Abe (1). Most of the previous wind-tunnel studies of stably stratified flows have been concerned only with the effect of stratification on turbulence intensity (4, 10). The reasons for this previous emphasis were that a

wind tunnel capable of creating flow with an adequately controlled density gradient had not been available and adequate field data for comparison of laboratory inversion-flow results had not been obtained.

Specifically, the objectives of the present study were:

1. determination of the optimum surface roughness, ambient wind speed, and thermal gradient in the approach flow to simulate prototype conditions,

2. determination of characteristic wind patterns over the 1:12,000 scale model,

3. comparison of wind-tunnel results with available prototype data, and

4. determination of the feasibility of simulating diffusion phenomena in the event satisfactory similitude is attained for the mean wind patterns.

## II. EXPERIMENTAL EQUIPMENT

### A. Wind Tunnel

The recirculating meteorological wind tunnel, driven by a 250 hp DC motor, contains an 88 ft long test section which is 6 x 6 ft in cross section. A 40 ft length of the test-section floor, beginning 32 ft from the upstream end, can be heated electrically or cooled by circulating brine through the floor. In addition, the ambient tunnel air can be heated or cooled by passing it over brine-chilled coils.

A set of fine screens reduces ambient turbulence to a level of about 0.1 percent. A trip fence (turbulence stimulator), located just upstream from the test section, serves to stabilize the flow pattern as well as to provide a thicker turbulent boundary layer than would exist without it. A complete description of the wind tunnel can be found in Ref. 3.

For this study a stabilized inversion flow was produced by heating the air and cooling the floor. A zero pressure gradient was maintained along the test section throughout all testing.

### B. Instrumentation

1. Hot-wire anemometer--A constant temperature hot-wire anemometer was used to obtain mean velocity measurements over a range of velocities from 0.3 to 7.0 ft/sec. The anemometer, constructed from tungsten-iridium wire, was $2 \times 10^{-5}$ in. in diameter

and approximately $4 \times 10^{-2}$ in. long. This element was mounted vertically so that it was perpendicular to the essentially horizontal flow patterns. Calibration of the wire at low speeds was made on a rotating arm mounted in a closed tank in which the speed of the rotating arm was calculated and compared to the hot-wire output. For larger flow velocities, a pitot tube and a "Transonic" pressure transducer were used.

2. Thermocouple--A copper-constantan thermocouple was used to measure mean temperatures. Output of the thermocouple was recorded on a Minneapolis-Honeywell single-channel recorder.

3. Smoke--Smoke was used to define the flow patterns for inversion flows which appeared above the surface of the model. Titanium tetrachloride was used to provide the dense smoke required for photographic purposes.

4. Surface flow patterns--Indicator paint was applied to the surface of the model to facilitate development of flow patterns. The paint consisted of white water-base latex paint mixed with congo red (an organic indicator of pH intensity). Diluted hydrochloric acid was applied to the painted surface which sensitized the surface to the presence of anhydrous ammonia. Anhydrous ammonia was then released from points of interest on the model surface into the air stream. A trace of the diffusion plume of ammonia, indicating the surface wind direction, showed as a pink streak on the blue background of the model.

5. Camera Equipment--During this study two cameras were used to record smoke and diffusion traces: (a) a series 100 Polaroid camera with integrating shutter utilizing both color and black and white films which allowed the results to be seen immediately, and (b) a speed-graphic camera utilizing 4 x 5 in. black and white film.

## C. Models

All the terrain models used in the study had as a base, one of the three 1:12,000 scale topographic models provided by the Navy. The plastic models were stiffened with plywood and fiberglass backing, and sand (0.0058 to 0.0116 in.) was glued to their surfaces to simulate natural roughness. The models were coated with indicator paint as previously described.

On the basis of preliminary wind-tunnel tests, the mountainous terrain east of the U. S. Naval Missile Facility appeared to influence the flow over the missile facility itself. In order that this influence might be included in the model flow, an extension of the model was constructed. The area included in the extended model is shown in Fig. 1. The same grid appears on Y & D drawing No. 949885, General Development Map, U. S. Naval Missile Facility, Point Arguello, California. The point locations are identical to those identified in Ref. 2.

# III. FLOW SIMILARITY

For flow patterns over the model in the wind tunnel to be representative of those in the prototype, similarity in the thermal characteristics of the flow as well as in the dynamic structure of the flow was required. Similarity arguments indicate three primary criteria must be satisfied before flow similarity can be expected. These criteria are geometrical similarity, Reynolds number similarity, and similarity in the approaching boundary-layer flows (including thermal and dynamic characteristics).

## A. Geometrical Similarity

Geometrical similarity was achieved through use of the 1:12, 000 scale model supplied by the Navy and through the extension mentioned in section II-C. The model scale was undistorted; i.e., the vertical and horizontal scaling were both at 1:12, 000.

## B. Reynolds-Number Similarity

If the Reynolds number is based on the ambient velocity U ft/sec, the height of a characteristic feature H ft, and the kinematic viscosity $\nu$ ft$^2$/sec, then typical values of Reynolds for prototype and model are

$$R_p = \frac{U_p H_p}{\nu_p} = \frac{(10)(2000)}{1.5 \times 10^{-4}} = 1.3 \times 10^8$$

and

$$R_m = \frac{U_m H_m}{\nu_m} = \frac{(10)(2000)}{(1.5 \times 10^{-4})(12000)} = 1.1 \times 10^4 .$$

In other words, the ratio $R_p/R_m$, when the same fluid, wind speed, and flow regime (either laminar or turbulent) are used for the model flow as are found in the prototype flow, becomes equal to the scale ratio -- 1:12,000 in this case.

For minimizing the apparent dissimilarity suggested by the large difference in $R_p$ and $R_m$, there are two distinct approaches available. When both flows are in the turbulent state over essentially flat surfaces, the model may be roughened to produce flow characteristics corresponding to those found at Reynolds numbers larger than the actual value. This approach depends upon producing flows in which the flow characteristics become constant (independent of Reynolds number) if a lower limit of the Reynolds number is exceeded. For example, the resistance coefficient for flow in a sufficiently rough pipe as shown in Schlichting (7, p. 521) is constant for a Reynolds number (mean flow speed x pipe diameter/kinematic viscosity) larger than $2 \times 10^4$. This implies that the basic flow quantity of surface shear stress $\tau_o$, is directly proportional to the mean flow speed squared $U^2$ times the fluid density $\rho$ -- $\tau_o \alpha \rho U^2$. Thus, if $\rho_m U_m^2 = \rho_p U_p^2$ for such flows, $\tau_{om} = \tau_{op}$. In turn, this condition is the necessary condition for

mean turbulence statistics such as root-mean-square values and correlation coefficients of the turbulence velocity components to be equal for the model and the prototype flow.

In the case where the laboratory flow speeds must be reduced to satisfy other similarity criteria (such as the thermal criteria described in the following section), the model flow may be actually laminar. When this happens, roughening of the model surface cannot produce the desired similarity between inertial and viscous forces (Reynolds number similarity of the type discussed previously). However, similarity between inertial and viscous forces may still be closely approximated. Basically the concept to use is that described by Abe (1) in which the turbulent prototype fluid is approximated by a fluid of molecular kinematic viscosity equal to an average turbulent eddy viscosity or kinematic turbulent exchange coefficient $K_M$. Then, a comparison of the Reynolds numbers $R_m$ and $(R_p)_{turb}$,

$$\frac{U_m H_m}{\nu_m} \text{ and } \frac{U_p H_p}{(K_M)_p} \text{ respectively,}$$

may be made for estimating the degree of dynamic similarity. The ratio of these two Reynolds numbers

$$\frac{R_m}{(R_p)_{turb}} = \left(\frac{U_m}{U_p}\right)\left(\frac{H_m}{H_p}\right)\frac{(K_M)_p}{\nu_m}$$

can be estimated by selecting typical values for the speed ratio $U_m/U_p$, the scale ratio $H_m/H_p$ (1:12,000 in this study), and the diffusivity ratio

$(K_m)_p/\nu_m$. Considering a velocity ratio of unity, a turbulent exchange coefficient of $2.3 \times 10^3$ cm$^2$/sec* and a kinematic viscosity for air of $2.3 \times 10^{-1}$ cm$^2$/sec, a very favorable value for the Reynolds number ratio is obtained:

$$\frac{R_m}{(R_p)_{turb}} = (1)\left(\frac{1}{1.2 \times 10^4}\right) 10^4 \simeq 1 .$$

The photographs of smoke-flow patterns (Figs. 10-37) show that flow conditions over the laboratory model were essentially laminar near the surface; however, flow downstream of the sharp ridges above the surface appears to be turbulent. This means that the type of Reynolds number similarity proposed in the preceding paragraph should be valid over a large part of the model. One should keep in mind, however, that $(K_m)_p$ is not really a constant; it varies both with height and location over the region, so that the Reynolds number ratio calculated is an average value having a representative order of magnitude.

In the upper region downstream from the ridges, similarity of flow is also expected on the basis of arguments presented in the second paragraph of this section. The argument need only be extended to include the invariance of flow with Reynolds number downstream from "sharp-edged" objects. To improve the similarity for this part of the flow, sand with a particle size range of 0.006 - 0.012 in. was cemented to the model surface. This selection of sand size was made on the basis

*Pasquill, F., Atmospheric Diffusion, D. van Nostrand Company Ltd., 1962, p. 72.

of geometric similarity for ridge features such as brush, trees and boulders which were estimated to have a mean height of 6 ft. Accordingly, $\frac{6 \times 12}{12000}$ gives a sand size of about 0.006 in.

C. Thermal Similarity

In the context of this study, vertical temperature gradients and the associated vertical density stratifications are of prime importance in determining the flow characteristics around various topographical features. If the modifications of vertical motion by atmospheric inversion are to be similar for the laboratory and the prototype flows, a criterion must be selected to insure adequate temperature variation over the wind-tunnel model. Several parameters could have been chosen, such as a Froude number or the Obukhov stability length; however, a Richardson number, as discussed by Sutton (9), was chosen because of its wide usage by meteorologists and because of its ease of evaluation as a bulk parameter.

The Richardson Ri number expressed as a local parameter is defined by

$$Ri = \frac{g}{\theta} \frac{\left(\frac{\partial \theta}{\partial z}\right)}{\left(\frac{\partial u}{\partial z}\right)^2} \quad .$$

When a bulk Richardson number is desired to describe the thermal influence over a layer of thickness $\Delta z$, the following form is

convenient:

$$Ri = \frac{g}{\theta} \frac{\Delta\theta}{(\Delta u)^2} \Delta z.$$

For the purpose of obtaining an estimate of Richardson number variation at Point Arguello at different heights, use was made of rawinsonde data taken over the 18 month period from July 1959 to December 1960. Richardson numbers were computed from monthly averaged profiles of temperature and wind speed taken at 500 ft layers from 500 to 5,000 ft and at 1,000 ft layers from 5,000 to 10,000 ft. The distributions of Richardson number obtained are shown in Fig. 2. The important observation to be made is, of course, that the atmosphere is nearly always stably stratified.

A typical calculation of the bulk Richardson number for the wind-tunnel flow is shown in Fig. 3. In this calculation, the layer over which Ri is calculated corresponds to the actual boundary-layer thickness for the flow.

Because the main interest in this study is in flow near the earth's surface, a bulk Richardson number for the layer 0 - 1,000 ft is of importance in comparing the effects of thermal stratification in the laboratory and prototype flows. Prototype data for 30 January 1964, were taken from Ref. 8 (pp. 17 and 22) to obtain a typical prototype Richardson number. The numerical evaluation gives the following

values for Ri (near station 1 mi):

$$(Ri)_p = \frac{9.81}{287} \frac{(3)}{(10)^2} 305 = 0.31 .$$

If thermal similarity is to exist for the model flow, a Richardson number $(Ri)_m$ for the corresponding layer should also be approximately equal to 0.31. Typical values over a 1 in.-thick layer for an ambient flow speed of 5 ft/sec and an overall temperature difference of 103°F (the maximum attainable at this speed) yield the following values for $(Ri)_m$:

$$(Ri)_m = \frac{32.2}{500} \frac{75}{(1.5)^2} \frac{1}{12} = 0.18 .$$

Although this value is about one-half that for the reference prototype flow, no major difference in model and prototype flow patterns was anticipated.

# IV. CHARACTERISTICS OF THE MODEL FLOW AND COMPARISON WITH THE PROTOTYPE FLOW

Having established that geometrical, dynamic and thermal similarity could be attained to a reasonable degree for a laminar flow in the model, a program of measuring and visualizing flows over the model was undertaken. Since inversion flows were of primary interest, the laboratory study was confined primarily to low-speed flow (5 ft/sec) with a maximum attainable temperature difference (the wind-tunnel floor was 103° F cooler than the ambient air). Flow patterns for the stable stratification were well documented in the cases of flow approaching from an azimuth of 315° and from 340°. These two directions were selected because they represent the most common flow directions for the prototype flow. Flow data for several different directions (305°, 315° and 325°) with no thermal stratification were obtained to determine flow-pattern differences for neutral and inversion flows.

## A. Boundary-Layer Characteristics Upwind from the Model

One of the first objectives of this study was to determine the nature of the boundary-layer flow approaching the model. The bulk Richardson number based on the thermal boundary layer gave an indication of the overall stability of the flow. As shown in Fig. 3, this

Richardson number for the inversion flow in the wind tunnel was approximately Ri = 0.34. For the lower 1,000-ft layer, the bulk Richardson number for the same flow was 0.18.

A detailed description of typical neutral and inversion velocity profiles is given by Fig. 4. In this figure, velocity profiles measured with a hot-wire anemometer are shown for both neutral and inversion flows with the ambient velocity near 5 ft/sec. Both profiles follow a power-law distribution of the form

$$u \propto z^{1/4}$$

where $u$ is the velocity and $z$ is the height above the floor. A power-law velocity distribution with this exponent is characteristic of low Reynolds number or nearly laminar boundary-layer flows. It can be noted from Fig. 4 that there is considerable scatter in data. These variations are the result of difficulty involved in measuring velocities in the low range necessary to establish a stabilized flow. For example, data were reproducible at a point in a single day to within about 20 percent for velocities below 2 ft/sec and to within about 10 percent for velocities above 2 ft/sec. Daily variations ranged up to 50 percent for low velocities and 20 percent for the higher velocity range. Because of these measurement difficulties, the flow speed was not reduced below 5 ft/sec in order to realize a larger value of the Richardson number.

A typical mean temperature profile is shown in Fig. 5. This profile depicts an inversion flow with an ambient velocity of 5 ft/sec. As can be seen, variations in temperature profiles were much smaller than for the velocity profiles. In a given day, temperature data were reproducible to within 1 - $2^0$ F. Indeed, temperature profiles for the approach flow appear to follow a power-law distribution.

## B. Temperature and Velocity Fields Over the Model

In order to compare wind-tunnel and field data better, twenty velocity and temperature profiles were taken along the lines shown in Fig. 6 at points 1 through 20. Figure 6 was used to show a comparison of wind-tunnel and field data. The data cross-section lines are identical to those indicated in Ref. 8. The ambient velocity approached the model along the $340^0$ azimuth which almost paralleled the principal data line. Reduction of data was performed to provide a ready comparison with the field data.

Lines of constant temperature are shown in Figs. 7 and 8. The constant temperature lines do not reflect the pronounced wave pattern seen in the lee of the ridge as was demonstrated by the field data (8, Fig. 5). Instead, a definite downward convergence of constant-temperature lines is apparent on the lee slope. The assumption that equi-temperature lines approximate flow lines may be accepted up to the highest point on the ridge. However, on the lee side, the flow

observed with smoke patterns was found to be so turbulent that no steady stream lines existed. The smoke dispersed so rapidly in the turbulent structure of the flow that photographs of the smoke patterns in the region on the lee slope were virtually impossible to obtain. Considerable mixing of the air in the lee of the ridge is apparent in the constant-temperature lines (Fig. 7) which are almost parallel to the floor for a considerable distance downstream and almost equally spaced in the vertical direction. The mixing was great enough immediately downwind from the ridge to melt the thin coating of ice which had formed everywhere on the 25° F floor. Figure 26 shows this melted region which indicates a strong downward convergence of air very close to the lee slope.

Lines of constant speed are shown in Figs. 9 and 10. The diagram of equal speed lines in Fig. 9 shows the rapid changes in the velocity field caused by the terrain features. It can be seen from Fig. 10 that the model causes an immediate change in the velocity field for the flow passing from the flat-plate approach flow to the flow over the model.

The changes of temperature and velocity along lines of constant elevation are shown in Figs. 11 and 12. The changes in temperature are seen to be inversely affected by the shape of the terrain. Furthermore, Fig. 11 shows that the surface temperature of the model itself was well above the 25° F temperature of the floor on which the model was resting. This temperature difference may aid in the establishment of

flow similarity since ground surface temperatures in the prototype would be expected to be somewhat higher than sea-surface temperatures. As expected, acceleration charted in Fig. 12 occurs on the upslopes where the flow is converging, while deceleration occurs on the downslopes where the flow is diverging. It is interesting to note, however, that an acceleration occurs just before the flow crosses offshore on the lee side and that this acceleration ends at all elevations just as the shoreline is reached. This region of acceleration may be caused by flow sweeping around the point in the pattern shown for observed smoke traces in Fig. 38.

A comparison of model and prototype temperature profiles was made in an attempt to establish at least some quantitative measure of similarity. Field data used in this comparison came from Smith, et al. (8, pp. 15-19). Figures 13 and 14 show two typical sets of field temperature profiles measured from the diagrams of potential temperature in Ref. 8. In these diagrams, $z$ represents elevation above the surface, $\delta$ represents boundary-layer thickness, $T_a$ represents the potential temperature at elevation $z$, $T_w$ represents surface temperature and $T_\infty$ represents the potential temperature of the ambient flow. Values of $\delta$, $T_w$ and $T_\infty$ were not given explicitly by Smith but were estimated for this study from the diagrams. The same value of $\delta$ (4, 000 ft) was used for all field profiles.

Figure 13 shows profiles for four sets of field data at a point corresponding to the location of the model-data-point number 16. Figure 14 shows profiles for four sets of field data at a point corresponding to the location of the model-data-point number 1. These figures, one upstream from Honda ridge and one downstream, show a basic similarity in the thermal structure for the prototype cases presented. Therefore, if the model data are compared to one set of field data, the comparison should be valid for the other cases. Also, if the prototype cases are typical of average field conditions, then the comparison of the model with one set of prototype data is a valid comparison under average prototype conditions.

Figures 15 and 16 compare wind-tunnel data with one set of field data for model-data-point numbers 1, 6, 10 and 16. Examination of the figures shows that even though there is not a quantitative agreement in the sense that the curves fall on top of each other, there is a similarity in the curve shapes and in the relative position of the curves for the different stations. This indicates that, as the flow crosses the terrain, the temperature field undergoes similar changes with both model and prototype. These similar changes indicate a similarity in flow patterns between model and prototype.

## C. Flow Patterns Over the Model

Two types of flow visualization techniques were used to obtain flow patterns. Photographs of surface flow directions using the

indicator paint on the model gave an indication of local flow directions at the surface. For example, Figs. 17 and 18 show typical examples of these flow patterns. Streaks such as those in Fig. 17 were produced by one release of ammonia at the upstream end of each streak. Patterns such as those in Fig. 18 were produced by a series of individual streaks placed head to tail in a downstream progression. Ambient flow for both figures is from top to bottom.

The best graphic description of the flow pattern above the surface was obtained by photographing smoke over the model. Figures 19 through 26 show smoke traces for an ambient flow direction of $340^0$, ambient velocity of 5 ft/sec and temperature difference of $115^0$ F. Figures 27 through 37 show smoke traces for an ambient flow direction of $315^0$, ambient velocity of 5 ft/sec and temperature difference of $115^0$ F. The photographs reveal a highly complex flow with interesting secondary flows produced by the ridge and valley system. Mean flow patterns were deduced from these photographs and dominant features were represented in graphic form on the topographic map.

Figures 38 and 39 show the basic flow patterns established with photographs of smoke and indicator paint streaks. The solid portions of the arrows indicate flow in which smoke released near the ground tended to stay close to the surface. The dotted portion of the arrows indicates where the flow -- once at the surface -- had separated and was somewhat above the surface. In general, for both flow directions, the smoke remained attached to the surface until the flow passed

over Honda Ridge, separated at the ridge line, and became turbulent downstream from the ridge. One notable exception is the flow with a $340^0$ ambient wind direction. In this case, the flow separated just before reaching Honda Canyon, passed over Honda Canyon, almost reattached on Honda Ridge, and separated in the lee of the ridge. In this particular case, flow occurred up Honda Canyon perpendicular to the main flow and below it. This effect can be noted in Figs. 19 and 26.

A second general observation was that, in a region east of Honda Ridge, the smoke tended to follow the course of the valleys. This effect is seen graphically in Fig. 39 and can also be noted in many of the other photographs. During testing it was noted that an air current ran parallel to the coast following the coast line south and curving east around the point toward the U. S. Naval Boathouse area. A small portion of this stream separated from the main stream and followed a course up Honda Canyon. This effect, in addition to the previously noted strong downward convergence along the lee slope, could cause high concentrations of material released to the north of Honda Canyon in the boathouse.

Figure 40 shows the model flow patterns for neutral flow with $315^0$ ambient flow direction. This flow differed from the inversion case in two significant factors. The flow did not tend to follow the terrain features as closely as did the inversion flow but followed a straighter course across the model. In addition, the flow did not tend to stay as near the surface or down in the valleys as did the inversion flow.

D. Diffusion Measurements

One set of tracer concentration measurements was made to determine the degree of similarity between diffusion in the laminar model flow and the corresponding turbulent prototype flow. Helium was used as a tracer for the model flow and was released from a point source in Hondo Canyon corresponding to a flourescent particle release point used in the field study as described in Ref. 8. In this case, the trajectory of the helium tracer and the flourescent particles were quite similar as can be observed in Fig. 32.

The helium used for the tracer gas was not pure but was mixed with air (90% air, 10% helium) to minimize buoyancy of the tracer. Concentration of the helium in the downwind plumes was measured at ground level along a line normal to the axis of the plume. Sampling points for these measurements are shown in Fig. 44. Mean concentration for the continuous point source was determined by means of a "Veeco" leak detector (model MS-9). A sample of the helium-air mixture was withdrawn from the flow by applying negative pressure to a hypodermic needle placed at the sampling point which was connected to a vacuum pump by means of plastic tubing. Figures 45-49 show how the concentrations varied across each cross section where measurements were made. From these data, a maximum concentration for a particular cross section can be determined.

A comparison of the relative rates of concentration decay with distance downwind from the model and the prototype sources is provided by the data shown in Fig. 50. The ordinate scales are arbitrarily matched for the model and the prototype data so that the data points are closely grouped. Of major interest are the slopes described by the data points. Although the prototype data show considerable scatter, the rates of decay appear to be essentially the same for the laboratory and field diffusion. This agreement is better than was anticipated since the laboratory flow was laminar while the field flow was turbulent -- however, both were stably stratified to approximately the same degree. An attempt to explain the agreement of the concentration decay rates under these conditions of flow is made in the following paragraphs.

In cases where the surface over which the flow occurs is irregular, composed of hills and valleys, dispersion of a passive additive to the atmosphere may be controlled primarily by strong spatial variation in convective transport by the mean motion. Especially in flows with strong stable thermal stratification is this mode of dispersion expected to be dominant. The significance of this possibility may be recognized most readily by examining the turbulent diffusion equation

$$\frac{\partial \overline{C}}{\partial t} + \overline{U}_i \frac{\partial \overline{C}}{\partial x_i} = \frac{\partial}{\partial x_i} \left( \eta \frac{\partial \overline{C}}{\partial x_i} - \overline{u_i c} \right)$$

When the mean flow is steady, a convectively dominated transport system would then be described by

$$\overline{U}_i \frac{\partial \overline{C}}{\partial x_i} = 0 .$$

Accordingly, the non-dimensional form for this conservation of mass statement is merely

$$\overline{U}'_i \frac{\partial \overline{C}'}{\partial x'_i} = 0 .$$

This implies, since no coefficients involving the scaling factors enter the equation, the only conditions necessary for similarity of the concentration field is that of geometrical similarity and mean velocity similarity in the vertical and, more importantly for rough terrain, in the horizontal which must be attained by meeting the conditions for dynamic similarity. Much work remains to establish the extent to which the foregoing arguments can be exploited for practical applications. The only known study of this nature is the exploratory work on simulation of mean winds and diffusion reported herein.

Although the type of similarity considered in this section appears to be based on radical simplifications, the results shown in Fig. 50 are sufficiently significant to warrant further research on this modeling concept. Satisfactory modeling techniques of this nature have great potential for the study of practical dispersion problems.

# V. CONCLUSIONS

As a result of the experimental work completed in the meteorological wind tunnel and the comparisons of these data with prototype data, the following conclusions can be made:

1. The meteorological wind tunnel is capable of producing inversion flows of sufficient intensity to model the inversion flows in the vicinity of Point Arguello and other coastal regions.

2. Comparison of wind-tunnel and prototype temperature data established at least a qualitative similarity in the structure of the model and prototype temperature field over the Point Arguello area.

3. Comparison of surface-flow directions and smoke traces for neutral and inversion flows established that excellent similarity exists in wind-flow patterns over the Point Arguello area and its model for inversion flows approaching from the northwest. Hence, use of a laminar laboratory flow to simulate a turbulent field flow over rough terrain under stable stratification is a modeling technique which appears to have considerable practical application.

4. When dispersion is dominated by convection due to highly non-uniform mean velocity fields, such as stably stratified flow over complex terrain, the laminar flow model can be used to predict rates of concentration decay downwind from steady continuous sources.

# BIBLIOGRAPHY


1. Abe, M., Mountain clouds, their forms and connected air currents, Part II, Bull. Central Met. Obs., Japan 7 (3), 1941.

2. Bankston, L., and Fast N., Observations of surface winds at Point Arguello, California and Vicinity, 8 through 16 May 1962, Technical Memorandum No. PMR-TM-62-10, Pacific Missile Range, Point Magu, California, 1962.

3. Cermak, J. E., and Plate, E. J., Micrometeorological wind-tunnel facility, Final Report, Contract No. DA-36-039-SC-80371, U. S. Army Electronic Research and Development Acitivity, Fort Huachuca, Arizona.

4. Ellison, T. H., Laboratory measurements of turbulent diffusion in stratified flows, Jour. Geophys. Res., 67, 3029, 1962.

5. Lettau, H. H., and Davidson, B., "Exploring the Earth's First Mile," Pergamon Press, New York, 1957.

6. Lyons, R., Panofsky, H. A., and Wollaston, S., The critical Richardson number and its implications for forecast problems, Jour. of Applied Meteorology, 3, 136, 1964.

7. Schlichting, H., "Boundary Layer Theory," Fourth Ed., McGraw-Hill, New York, 1960.

8. Smith, T. B., et al., Micrometeorological investigation of Naval Missile Facility, Point Arguello, California, Final Report on Contract N123 - (61756) 32885 A (PMR), 2 Vols., 31 July 1964.

9. Sutton, O. G., "Micrometeorology," McGraw-Hill, New York, 1953.

10. Wiskind, H. K., A uniform gradient turbulent transport experiment, Jour. Geophys. Res., 67, 3033, 1962.

# BIBLIOGRAPHY


1. [illegible]

2. [illegible]

3. [illegible]

4. [illegible]

5. [illegible]

6. [illegible]

7. [illegible]

8. [illegible]


# FIGURES

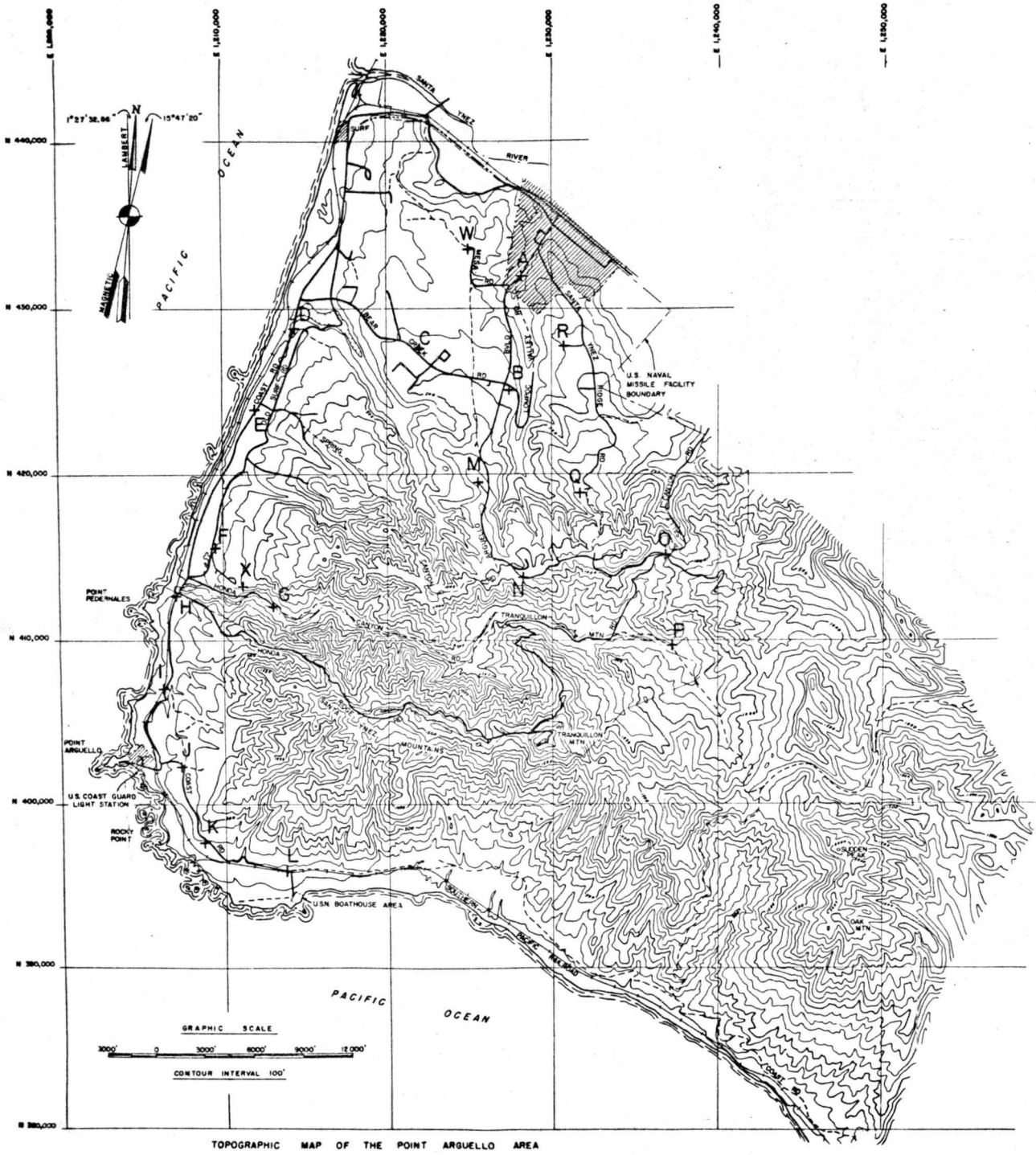


TOPOGRAPHIC MAP OF THE POINT ARGUELLO AREA

Fig 1 Topographic map of the model of Point Arguello, California

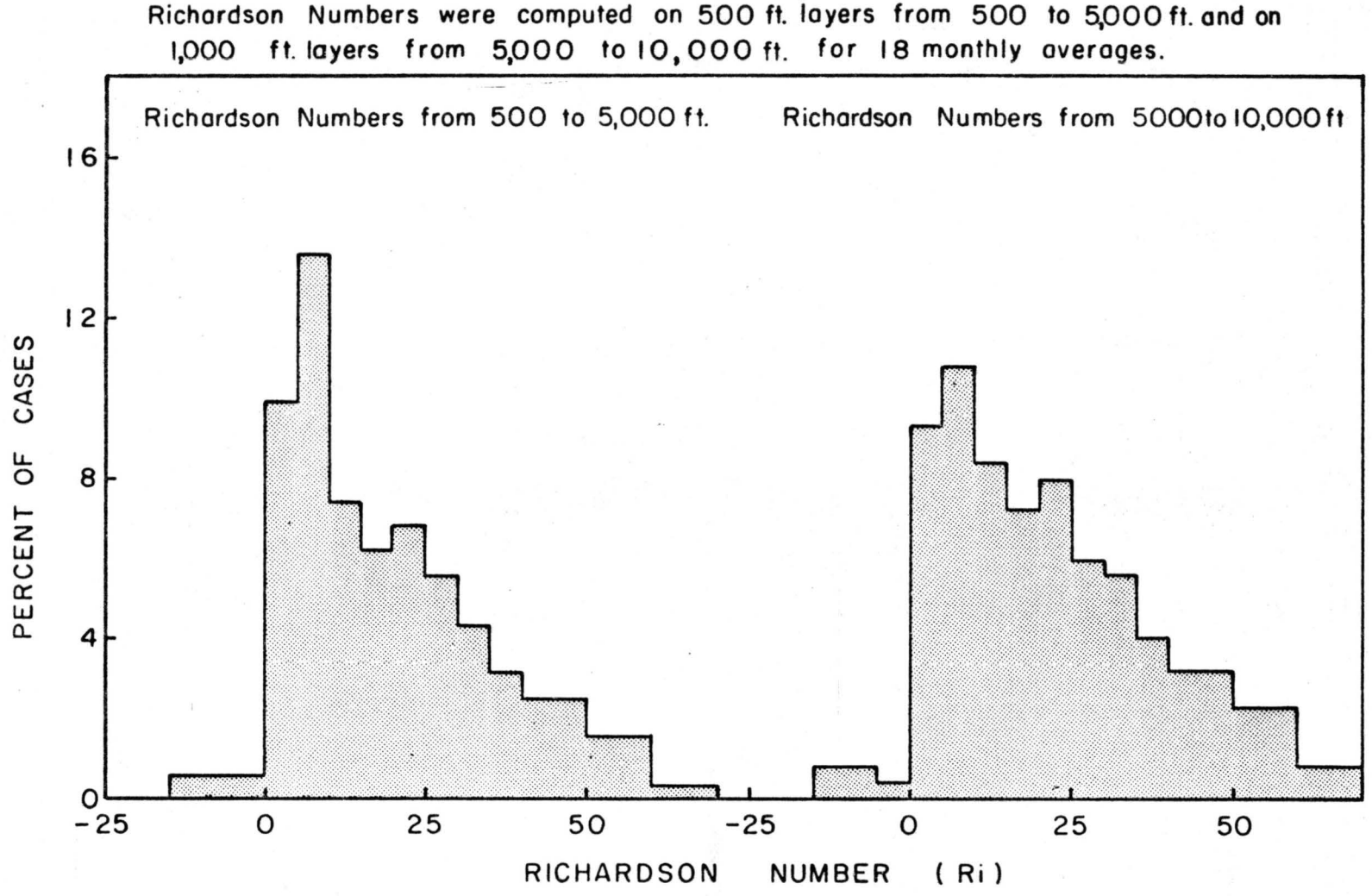


Fig 2 Distribution of Richardson numbers for Point Arguello, California

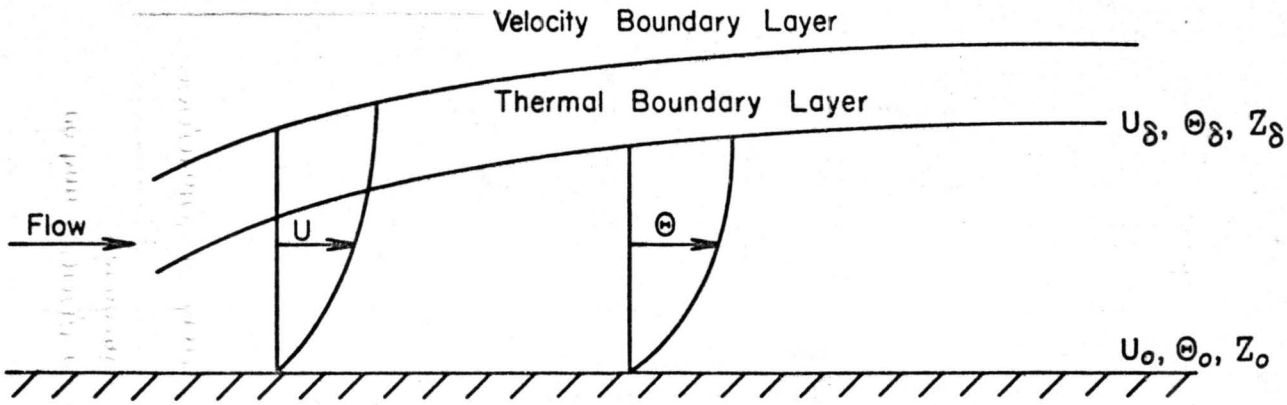


$$R_i = \frac{g\left(\frac{\partial \Theta}{\partial Z}\right)}{\Theta\left(\frac{\partial U}{\partial Z}\right)^2} \qquad \text{but} \quad \frac{\partial \Theta}{\partial Z} \cong \frac{\Theta_\delta - \Theta_o}{Z_\delta - Z_o} \qquad \frac{\partial U}{\partial Z} \cong \frac{U_\delta - U_o}{Z_\delta - Z_o}$$

$$R_i \cong \frac{g}{\Theta_{av}} \frac{(\Theta_\delta - \Theta_o)(Z_\delta - Z_o)}{(U_\delta - U_o)^2}, \quad \text{where } \Theta_{av} = \frac{\Theta_\delta + \Theta_o}{2}$$

Data for Wind Tunnel Flow Approaching the Model

$\Theta_\delta = 128^\circ F = 588^\circ R$, $\Theta_o = 25^\circ F = 485^\circ R$, $\Theta_{av} = 76.5^\circ F = 536.5^\circ R$

$Z_\delta = 13.5'' = 1.12'$, $Z_o = 0$ $\qquad$ $U_\delta \cong 4.5$ fps, $U_o = 0$

$$R_i \cong \frac{g}{\Theta} \frac{(\Theta_\delta - \Theta_o)(Z_\delta - Z_o)}{(U_\delta - U_o)^2} \cong \frac{32.2}{536.5} \frac{(103)(1.12)}{(4.5)^2}$$

$R_i \cong 0.34$

Fig. 3 Bulk Richardson number for boundary layer flow

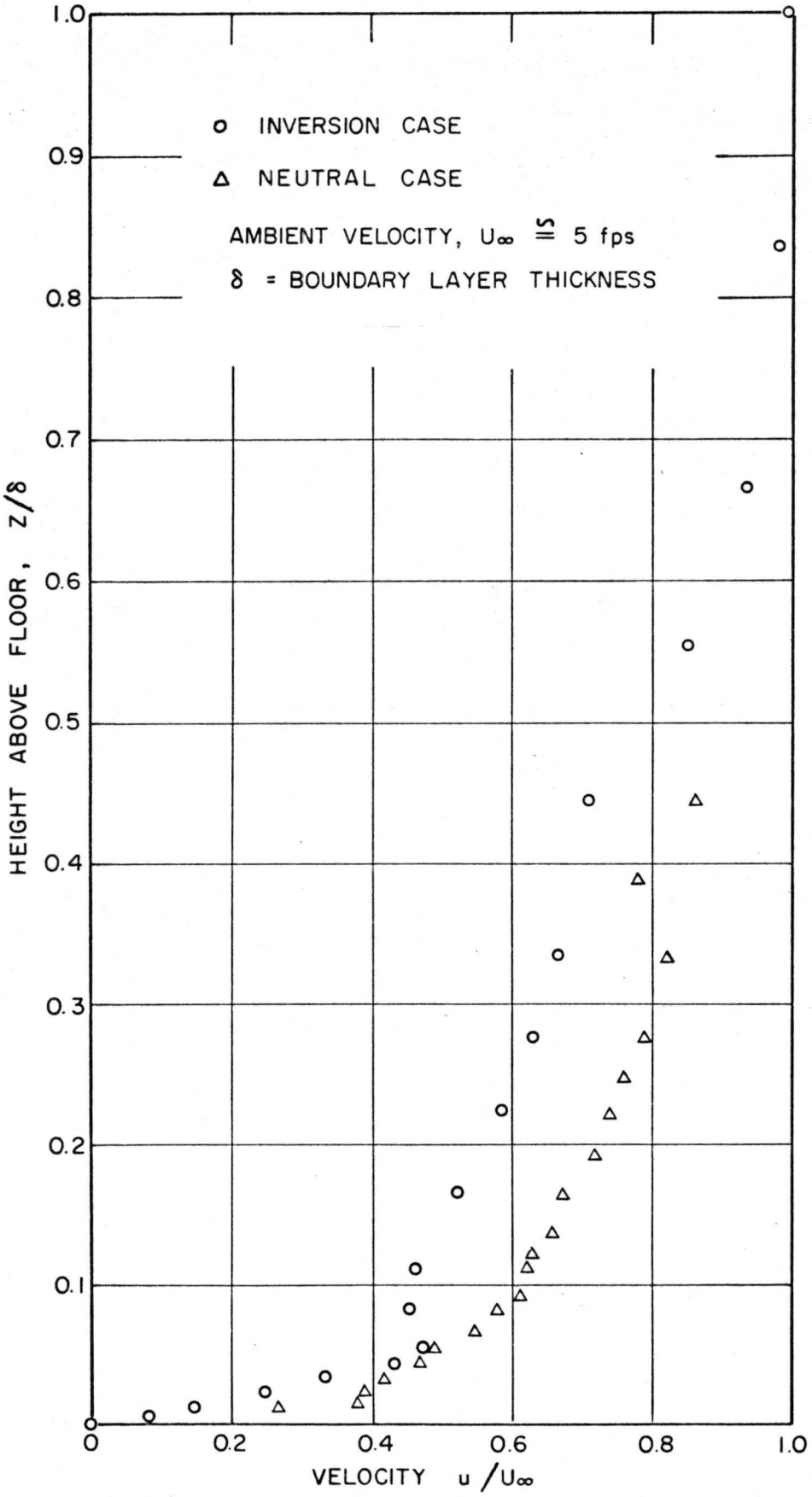


Fig. 4 Typical approach flow velocity profiles

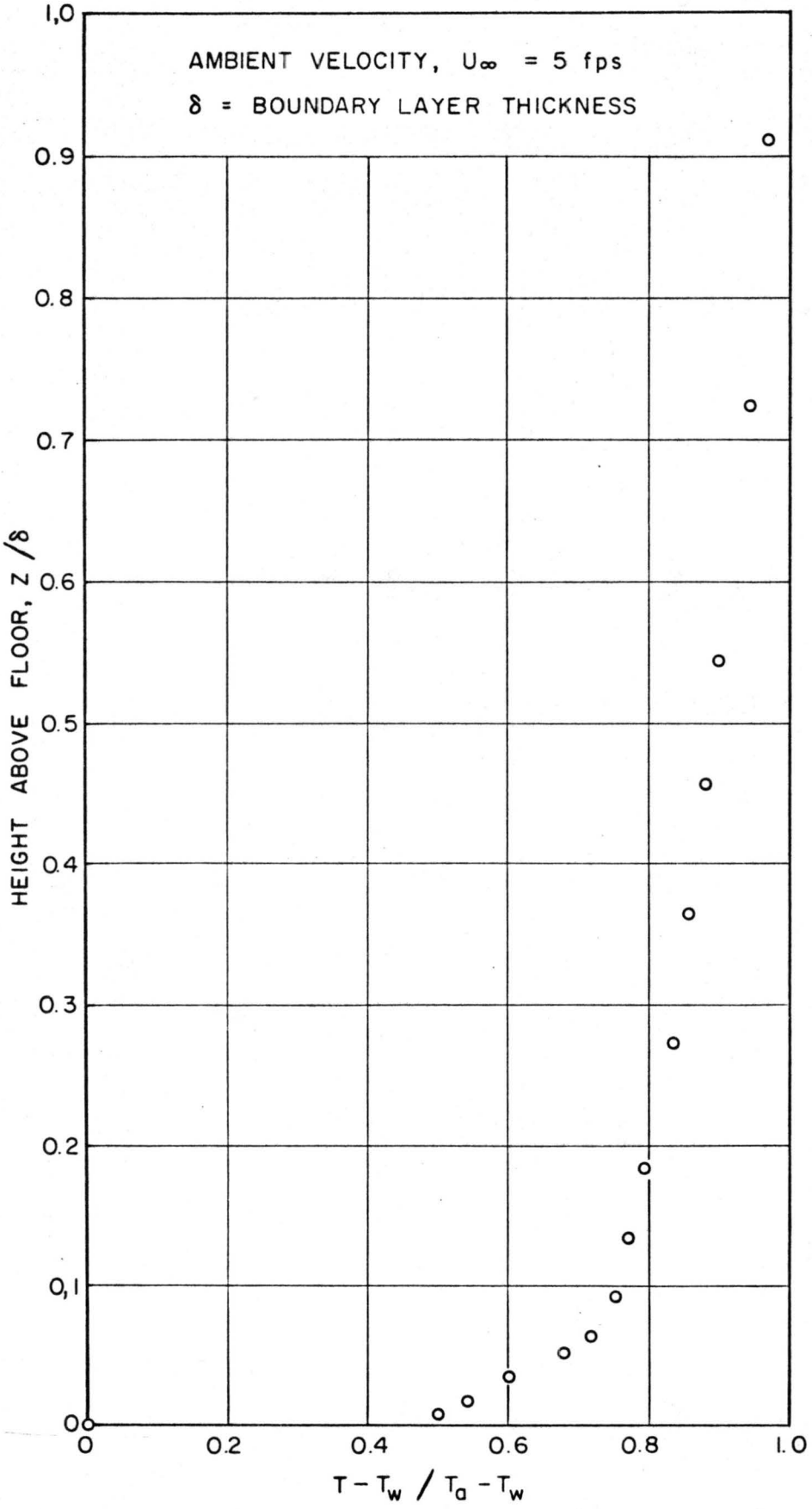


Fig. 5 Typical approach flow temperature profile

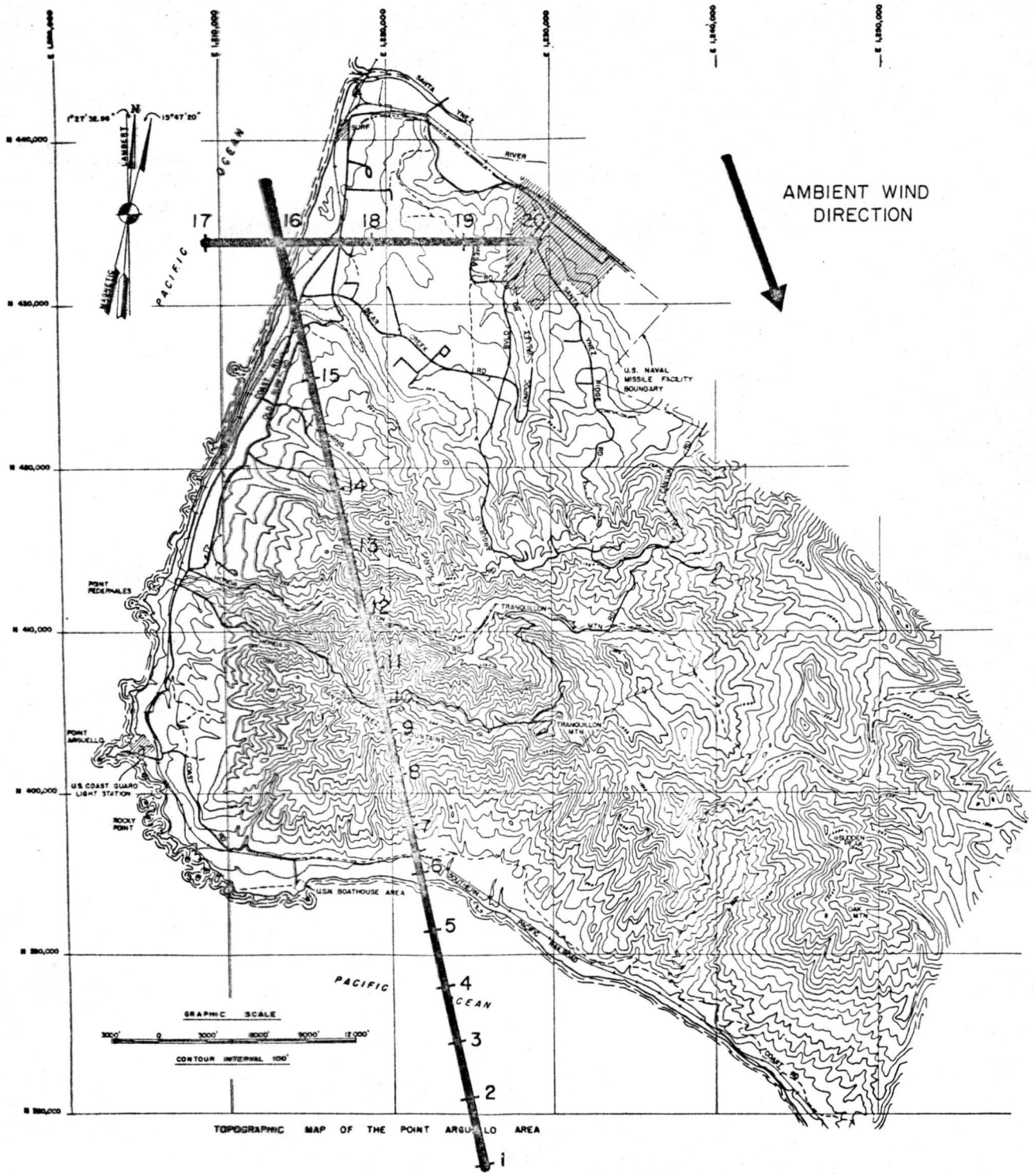


Fig. 6 Model of Point Arguello showing data cross section lines

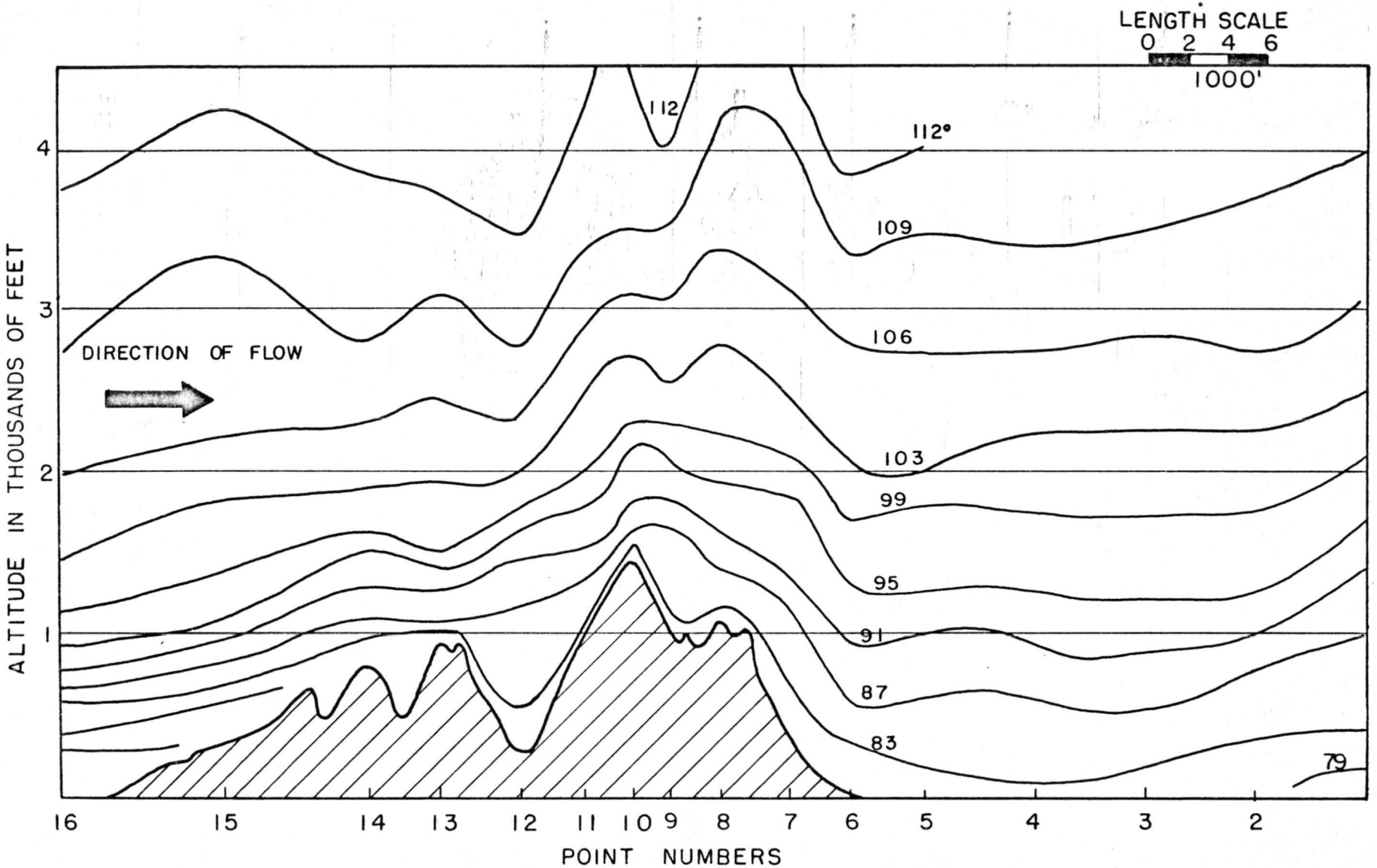


Fig. 7 Vertical cross section showing constant temperature lines

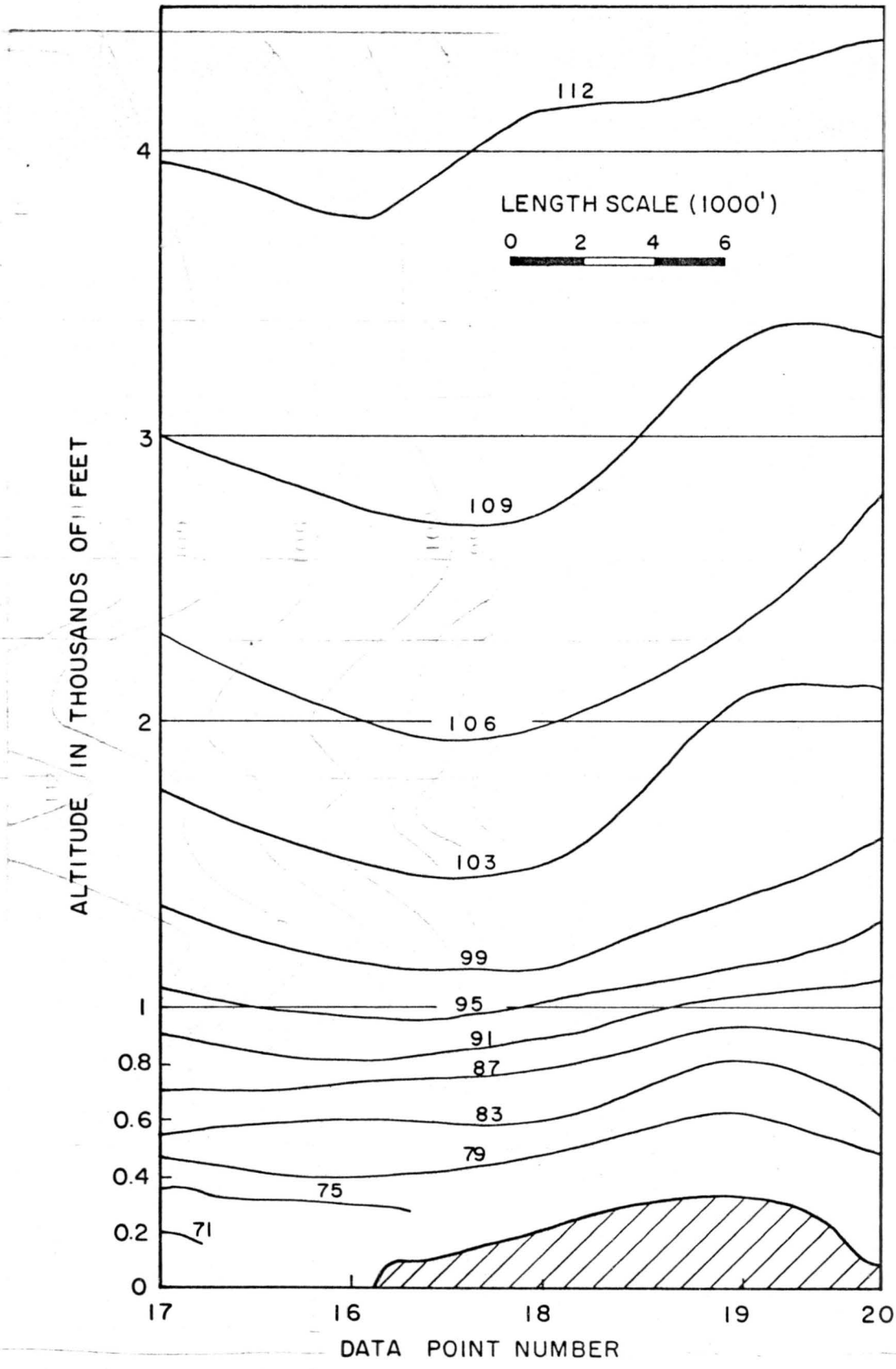


Fig. 8 Vertical cross section showing constant temperature lines

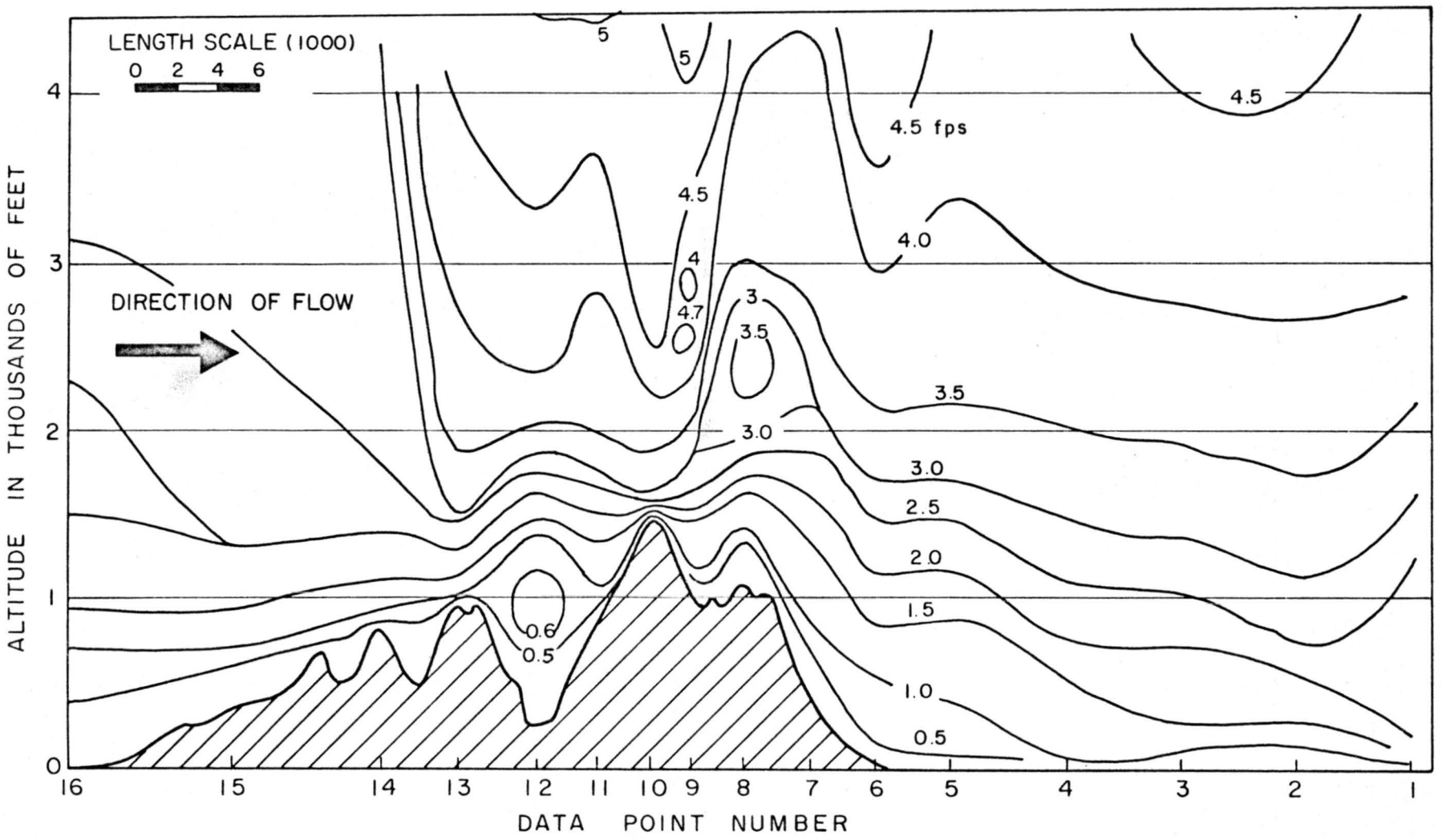


Fig. 9 Vertical cross section showing constant velocity lines

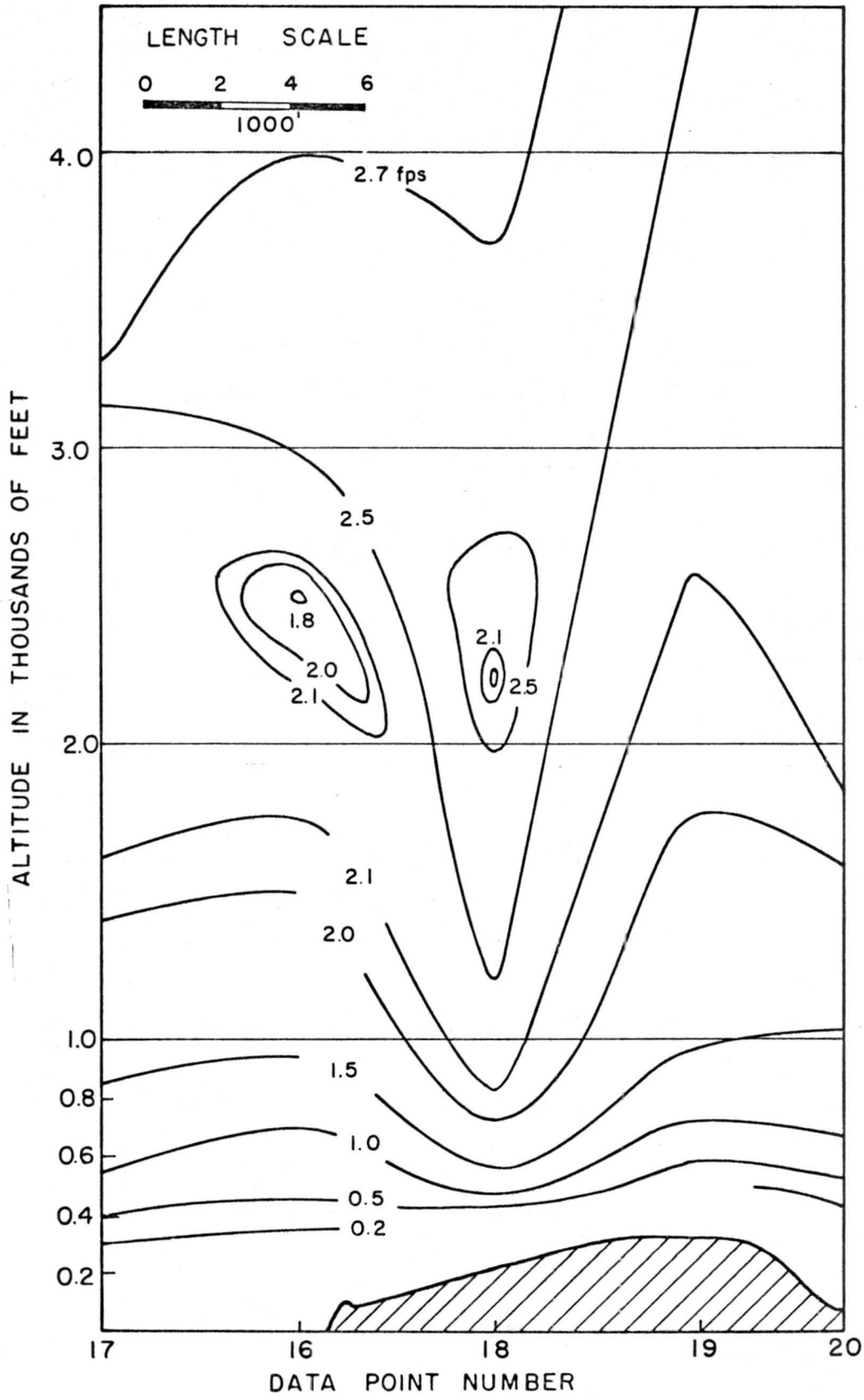


Fig. 10 Vertical cross section showing constant velocity lines

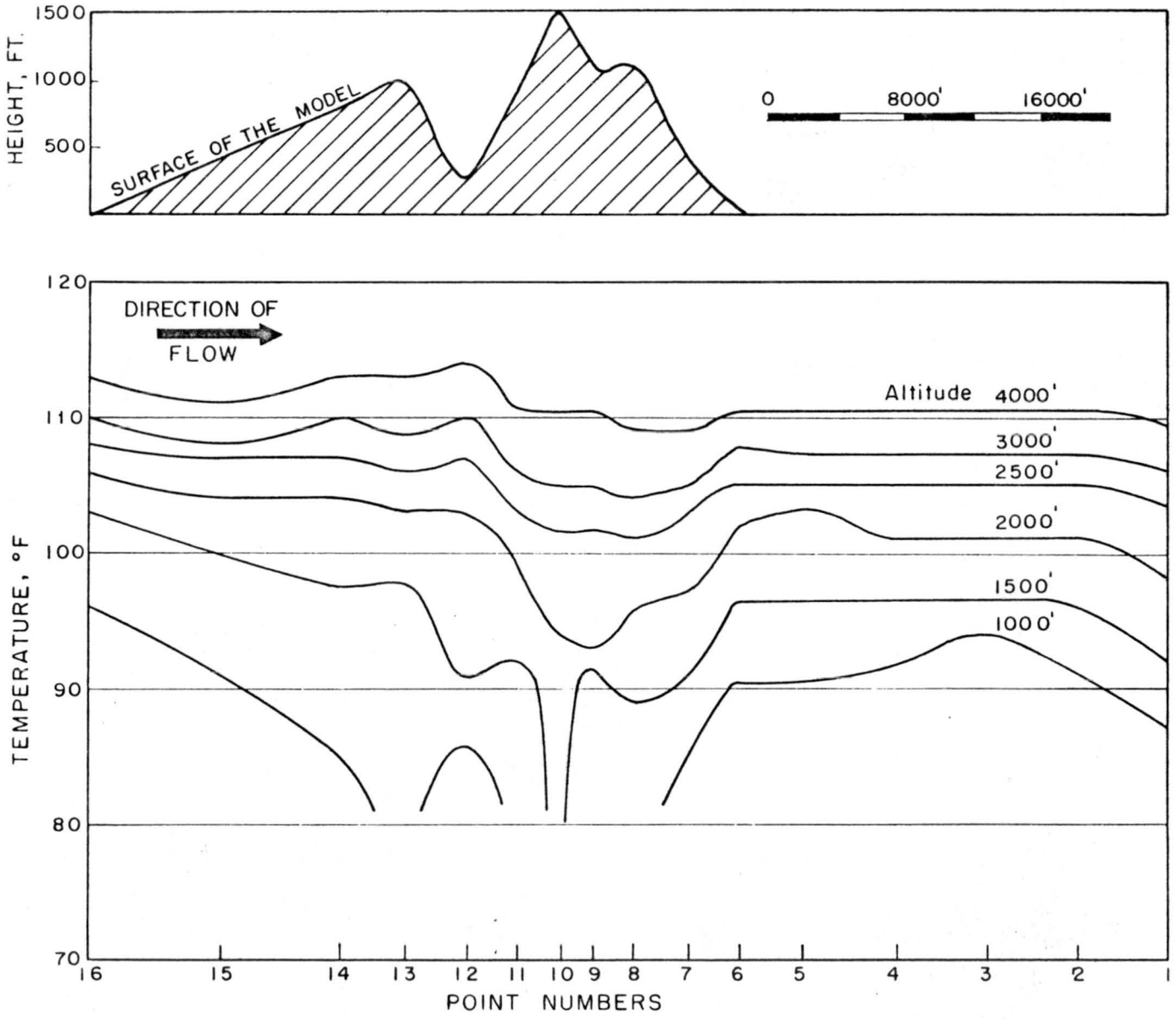


Fig. 11 Temperature variations at constant elevations

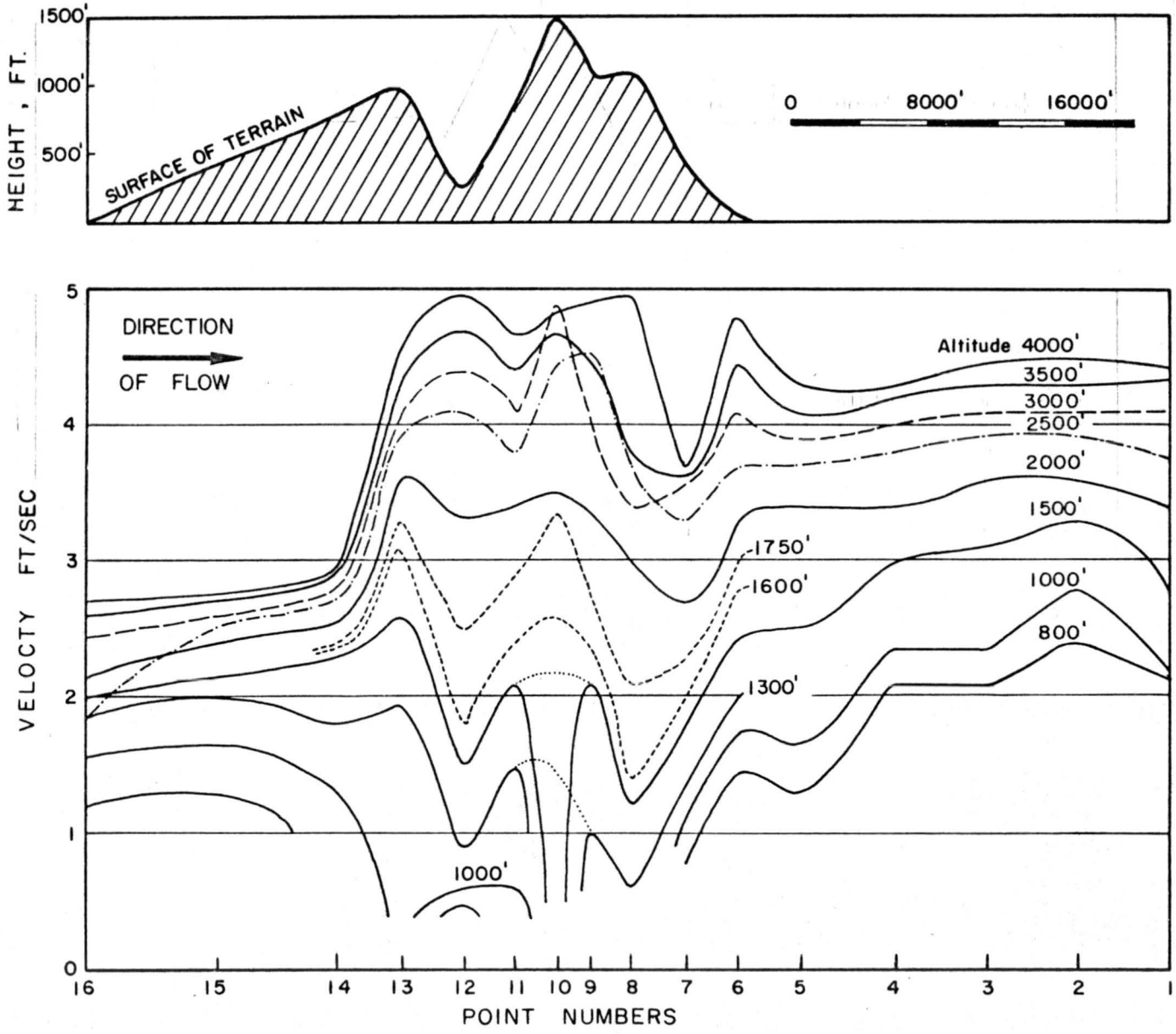


Fig. 12 Velocity variations at constant elevations

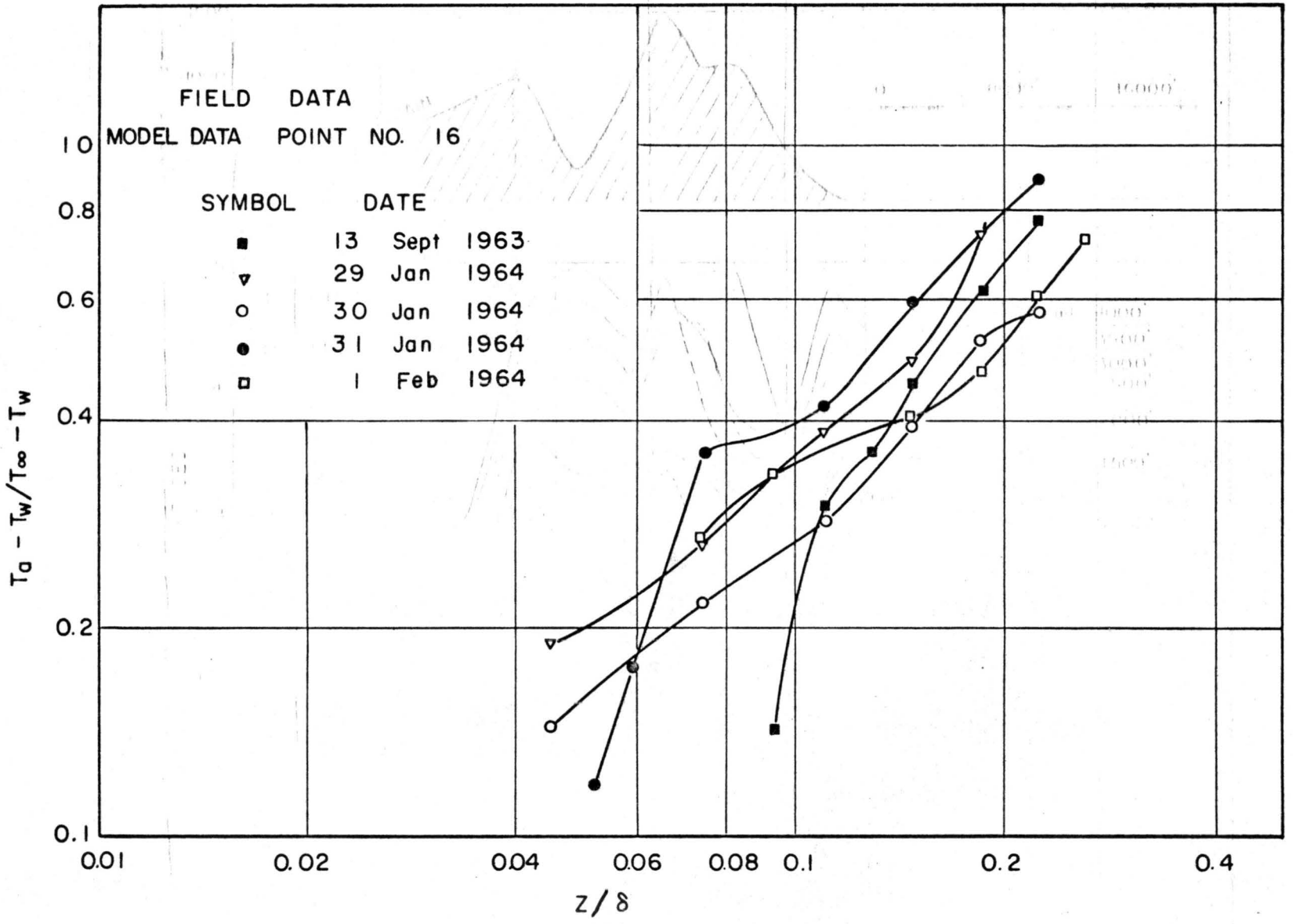


Fig. 13 Non-dimensional temperature profiles for field data

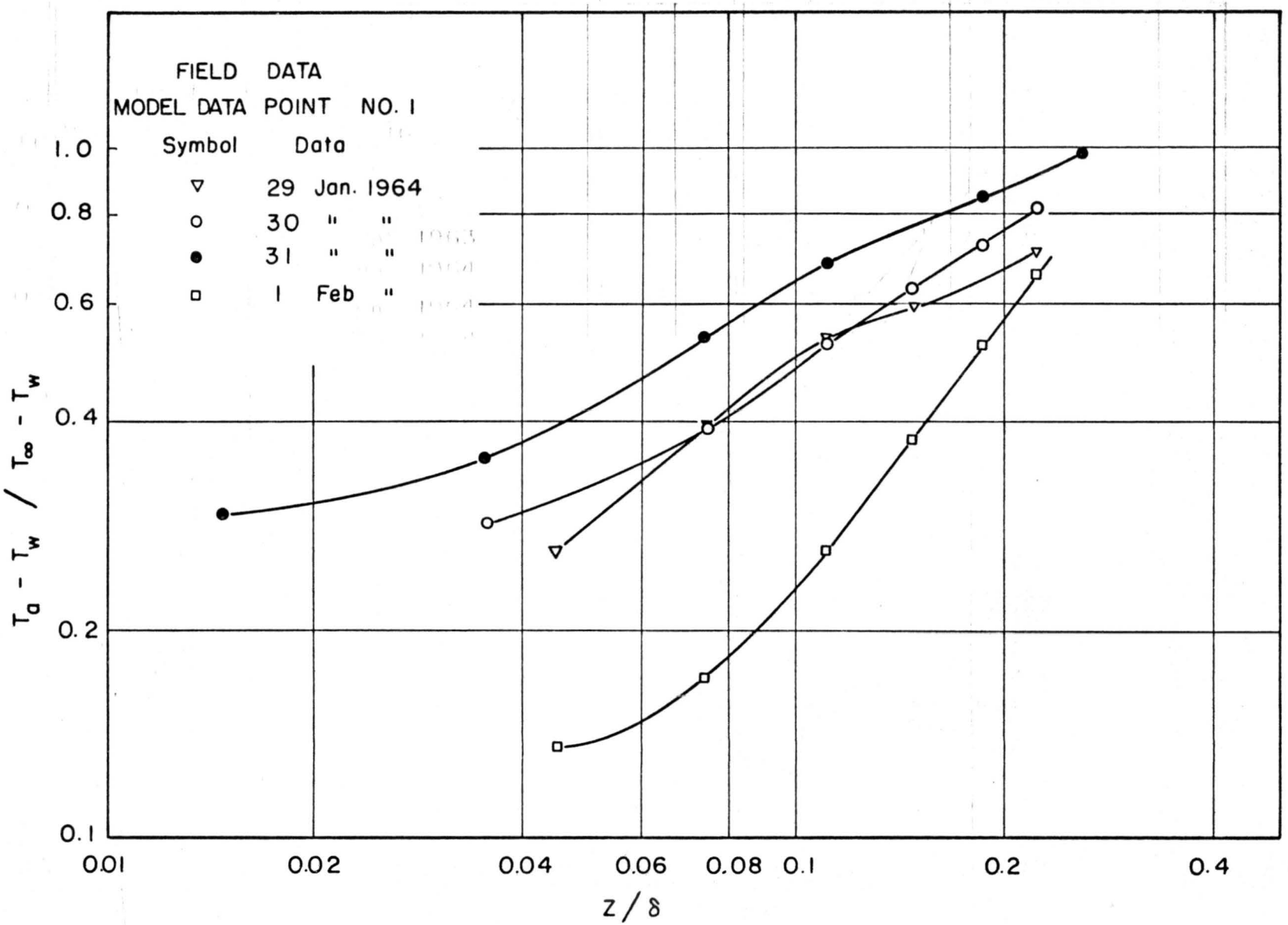


Fig. 14 Non-dimensional temperature profiles for field data

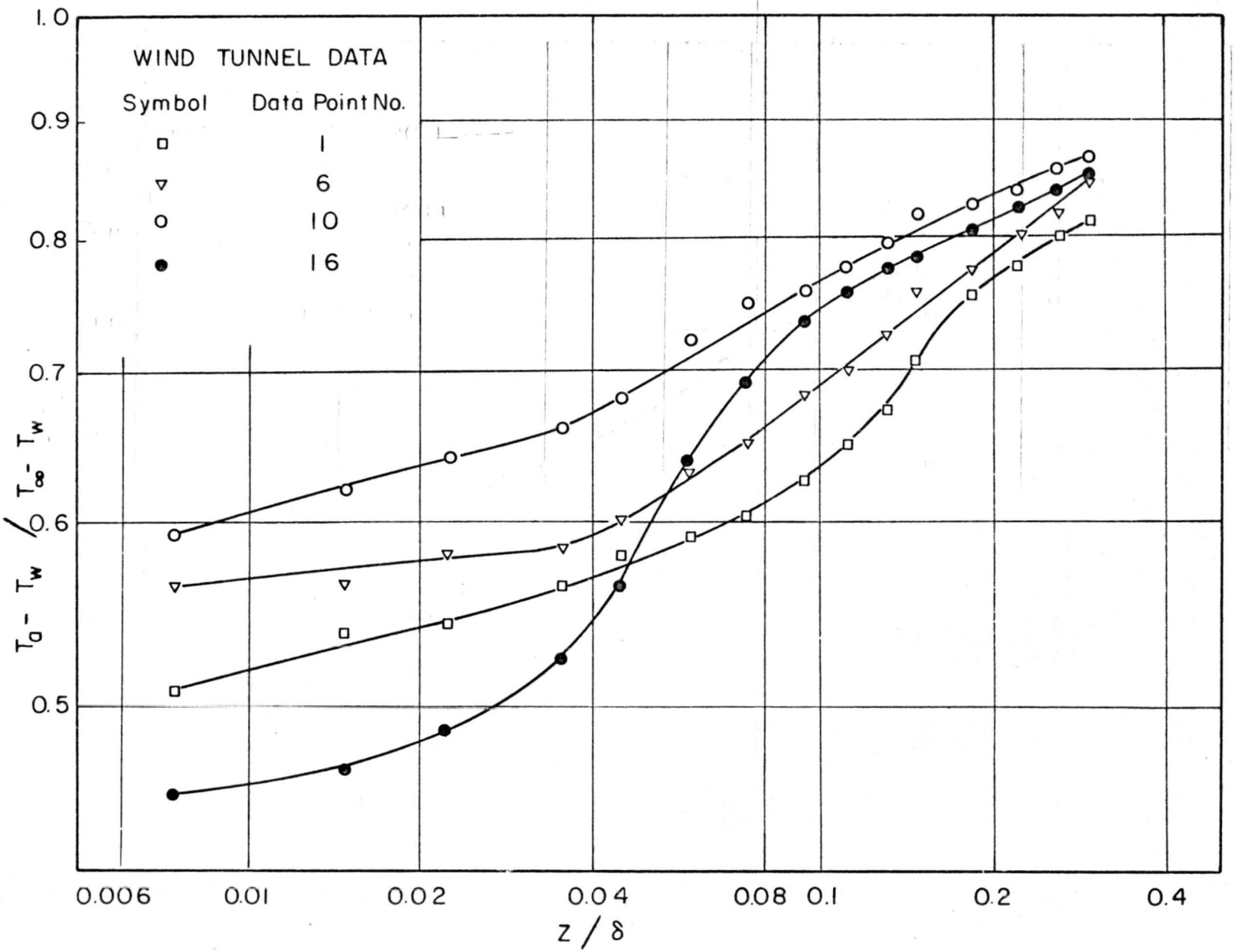


Fig. 15 Non-dimensional temperature profiles for wind tunnel data

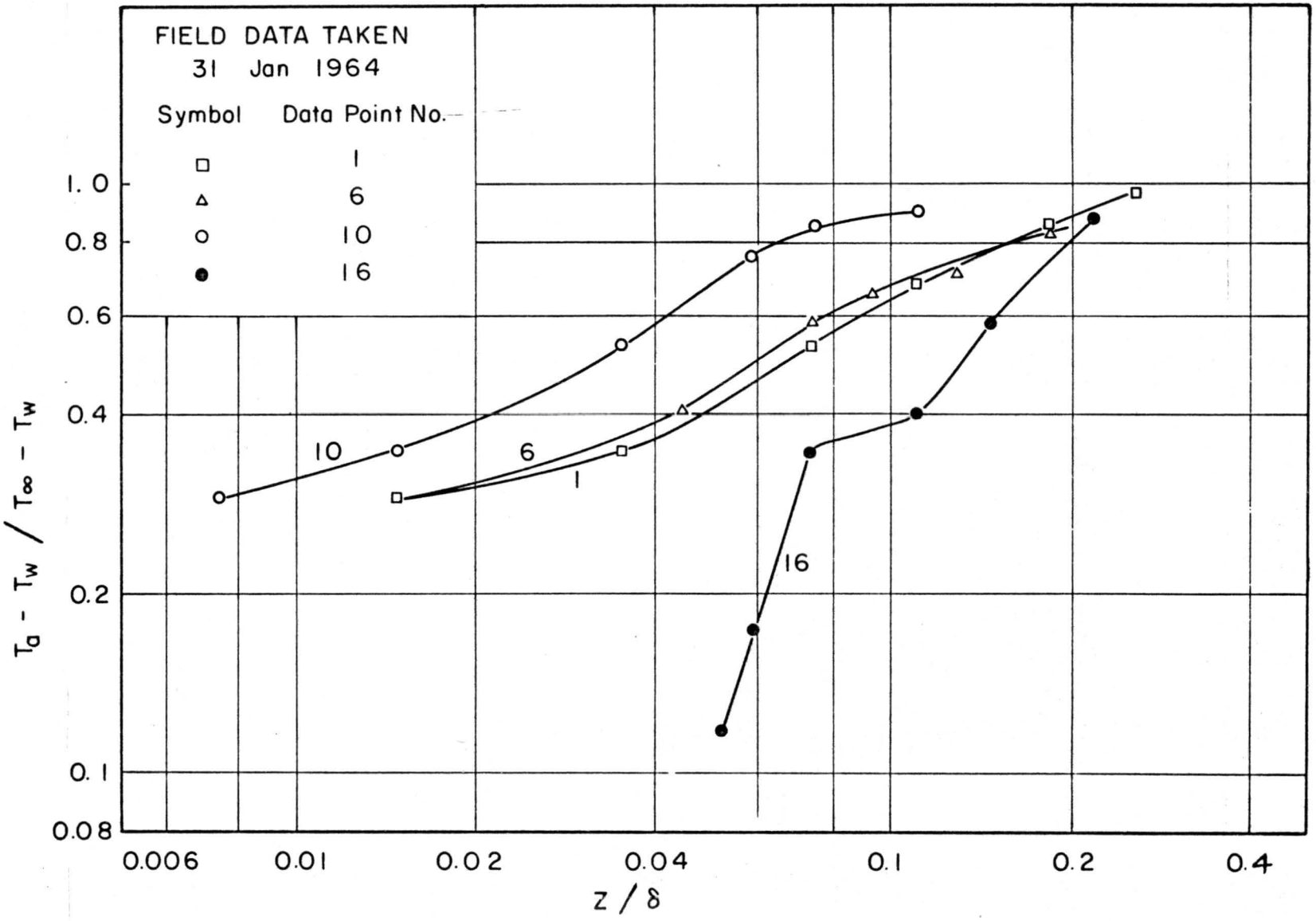


Fig. 16 Non-dimensional temperature profiles for field data

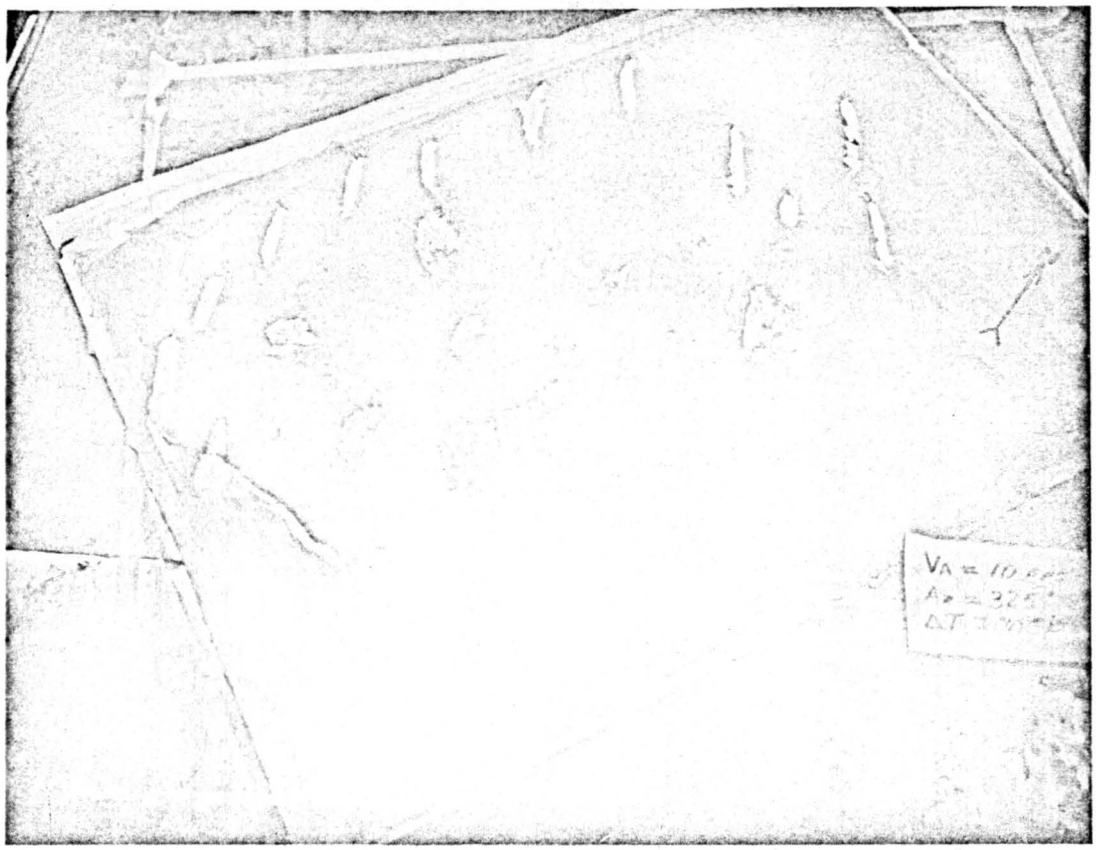

Fig. 17 Single release ammonia trace data

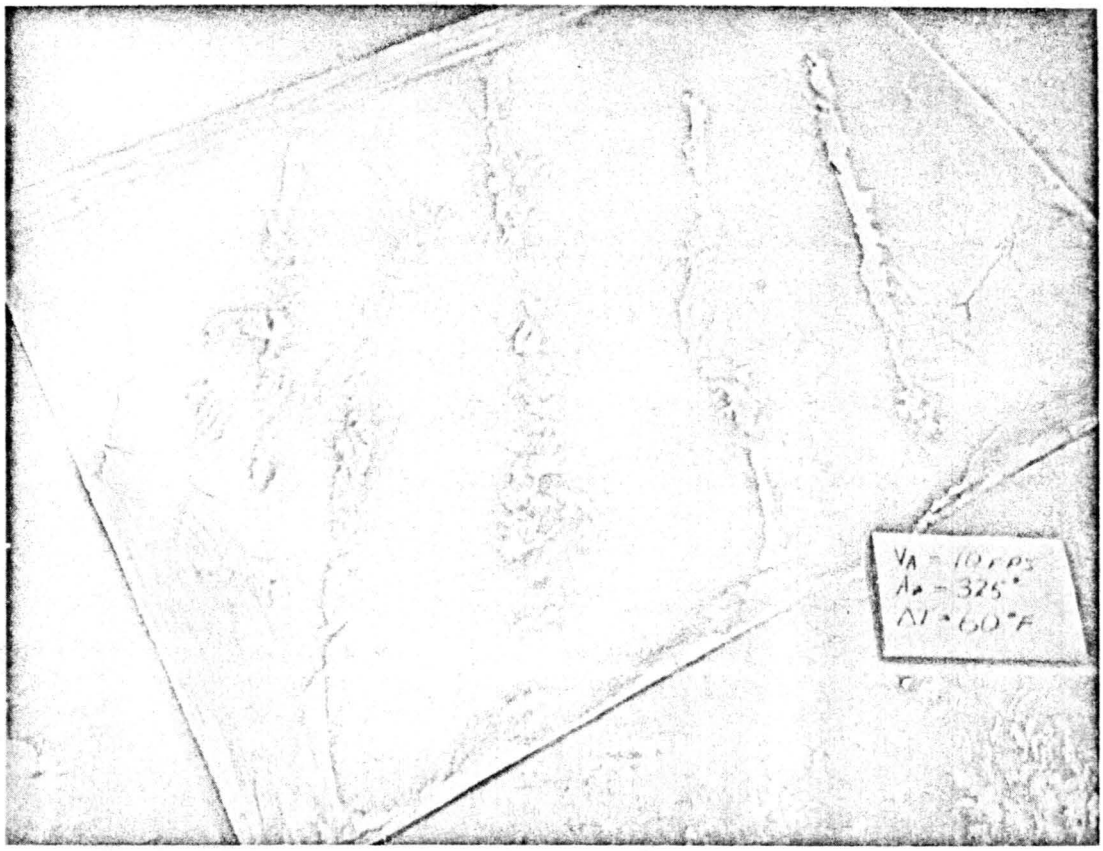


Fig. 18 Multiple release ammonia trace data

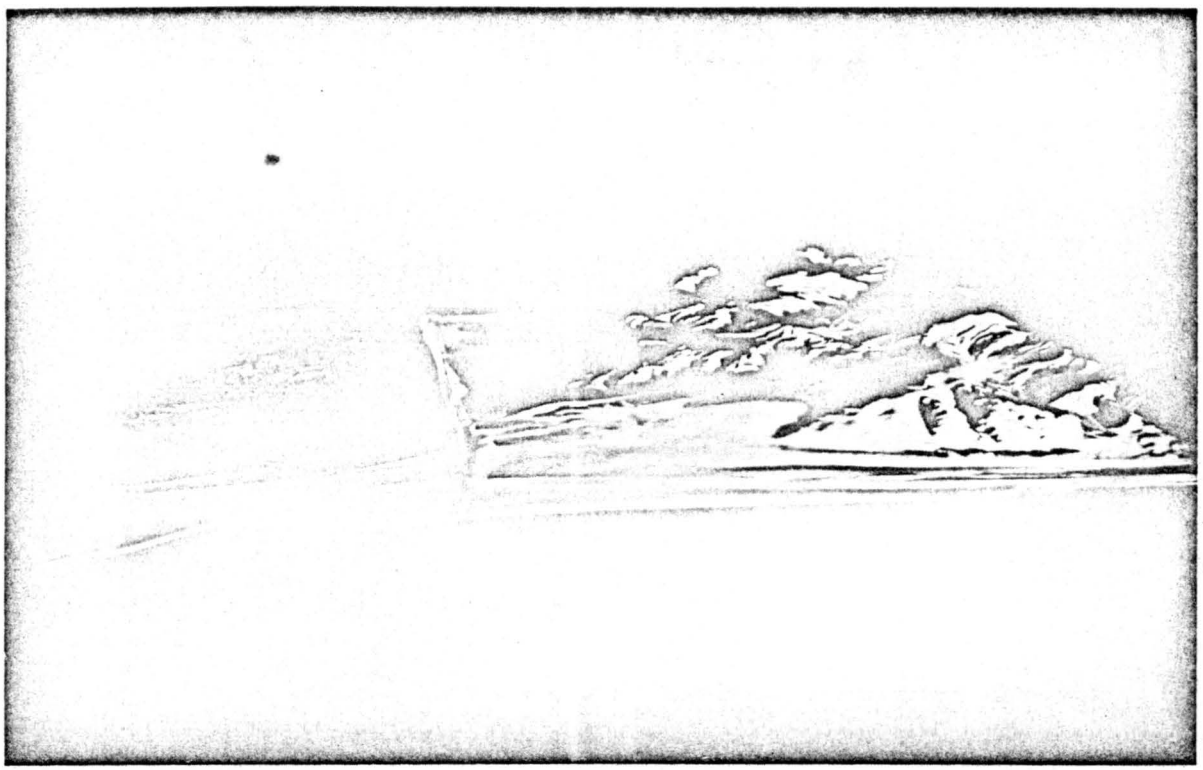

Fig. 19 Smoke flow patterns for $340^0$ ambient flow direction

Fig. 20 Smoke flow patterns for $340^0$ ambient flow direction

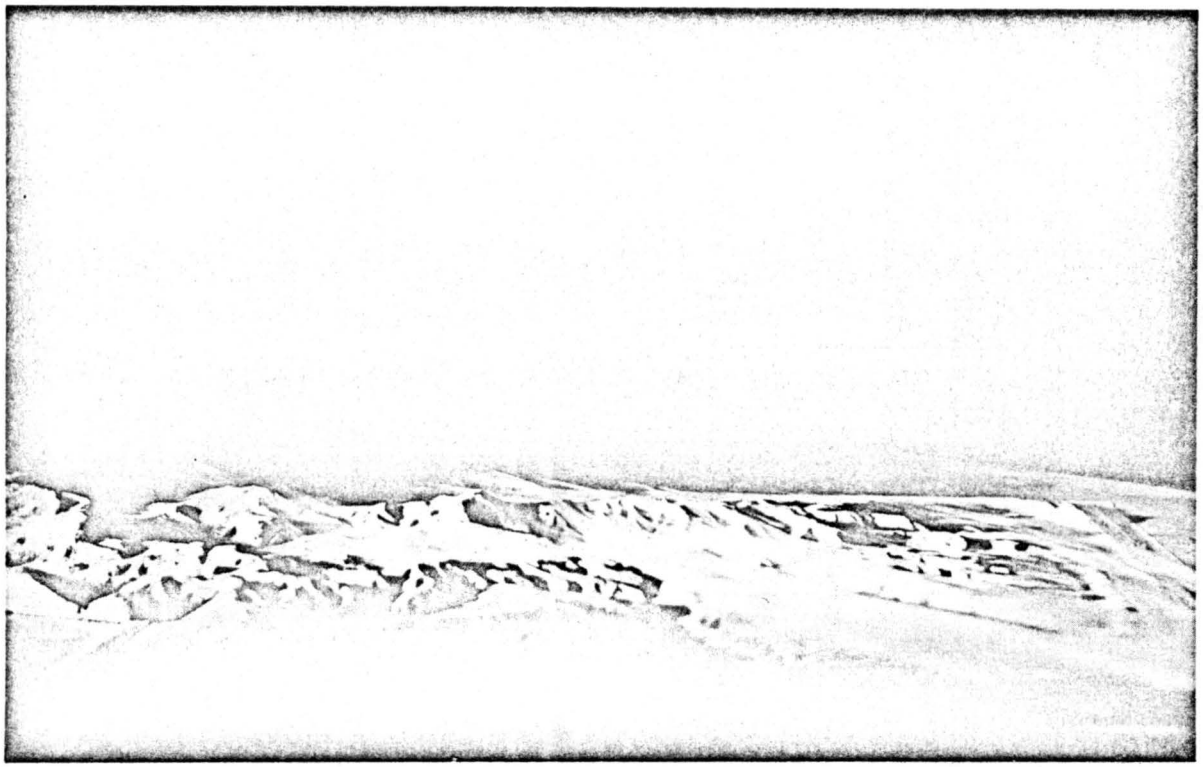

Fig. 21 Smoke flow patterns for $340^0$ ambient flow direction

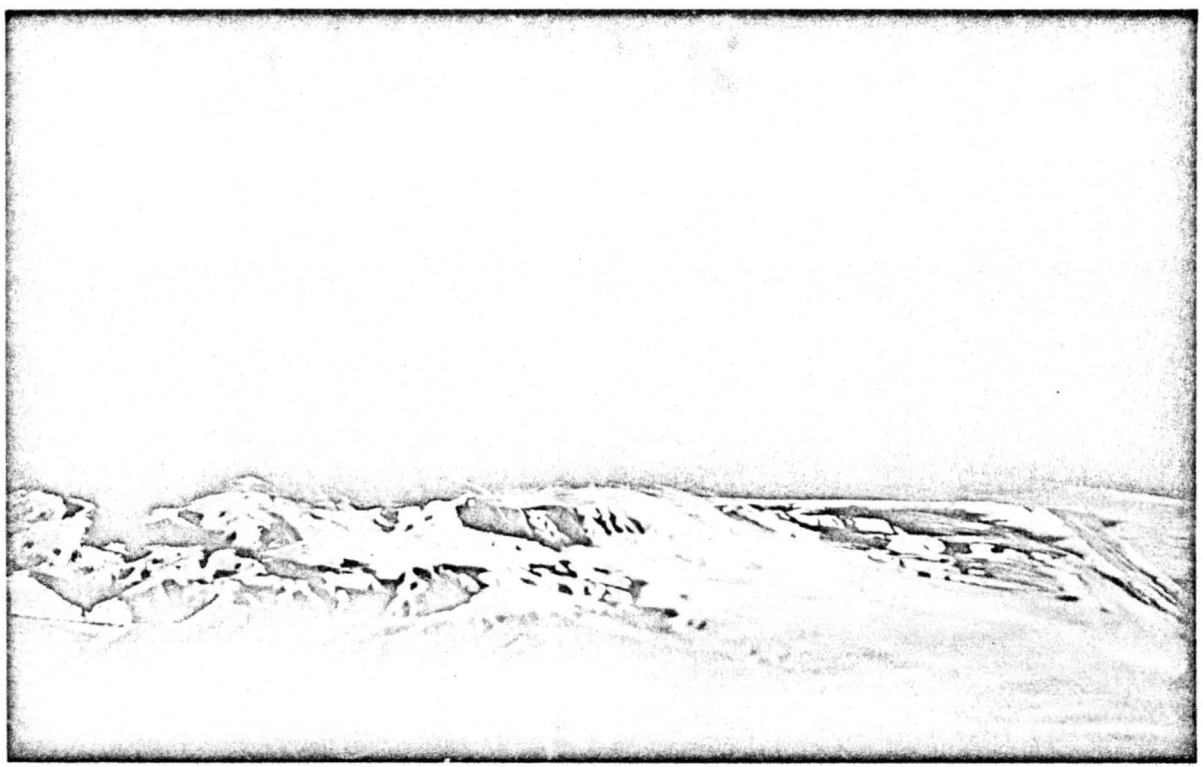

Fig. 22 Smoke flow patterns for $340^0$ ambient flow direction

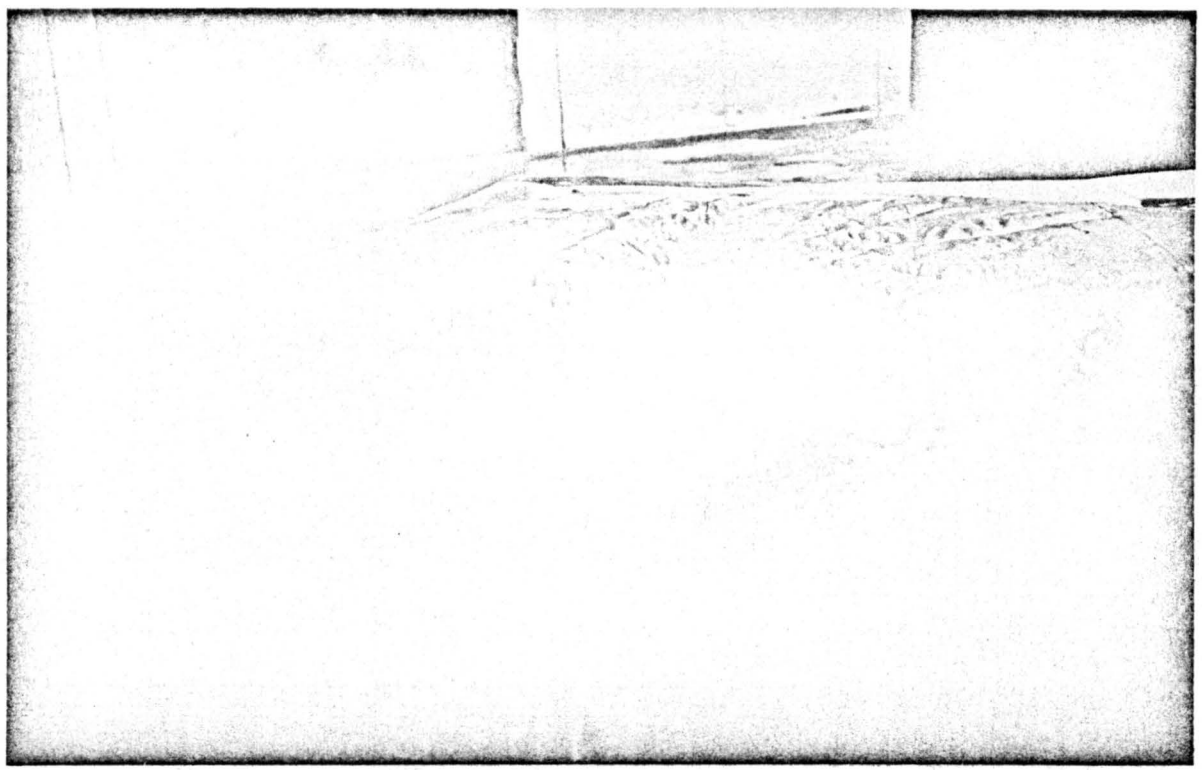

Fig. 23 Smoke flow patterns for $340^0$ ambient flow direction

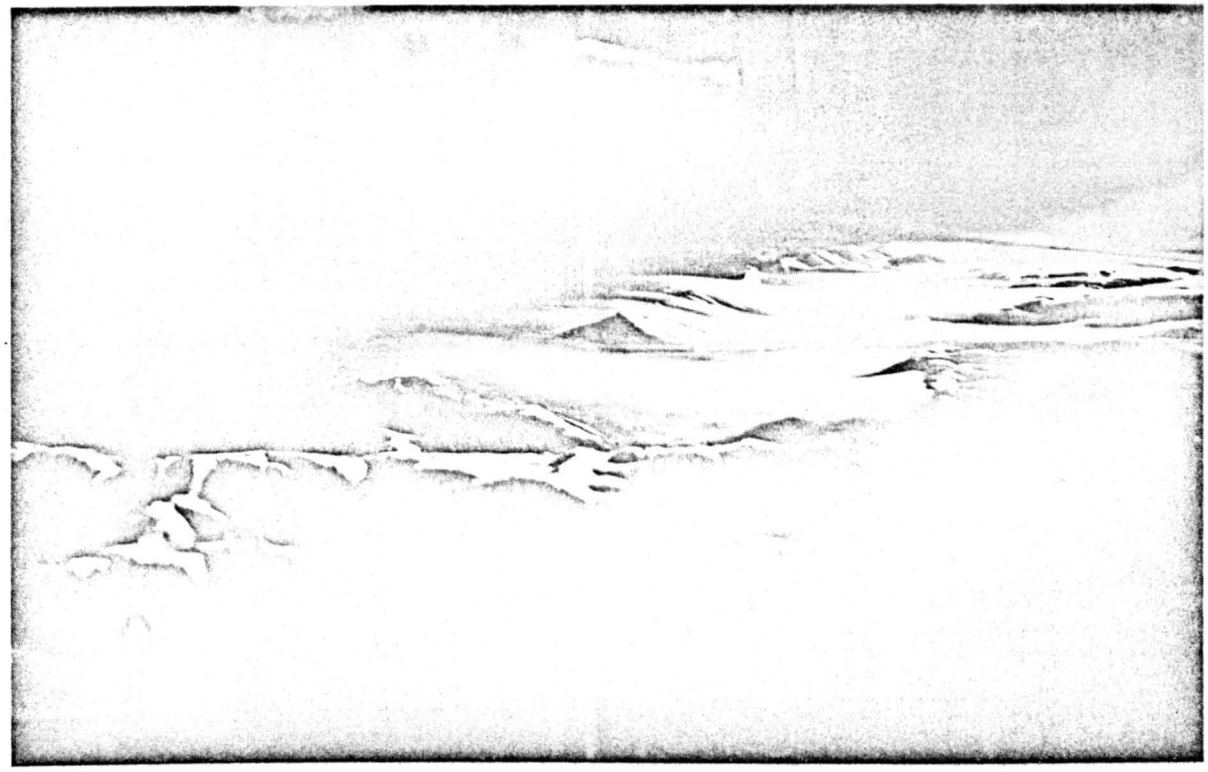

Fig. 24 Smoke flow patterns for $340^0$ ambient flow direction

Fig. 25 Smoke flow patterns for $340^0$ ambient flow direction

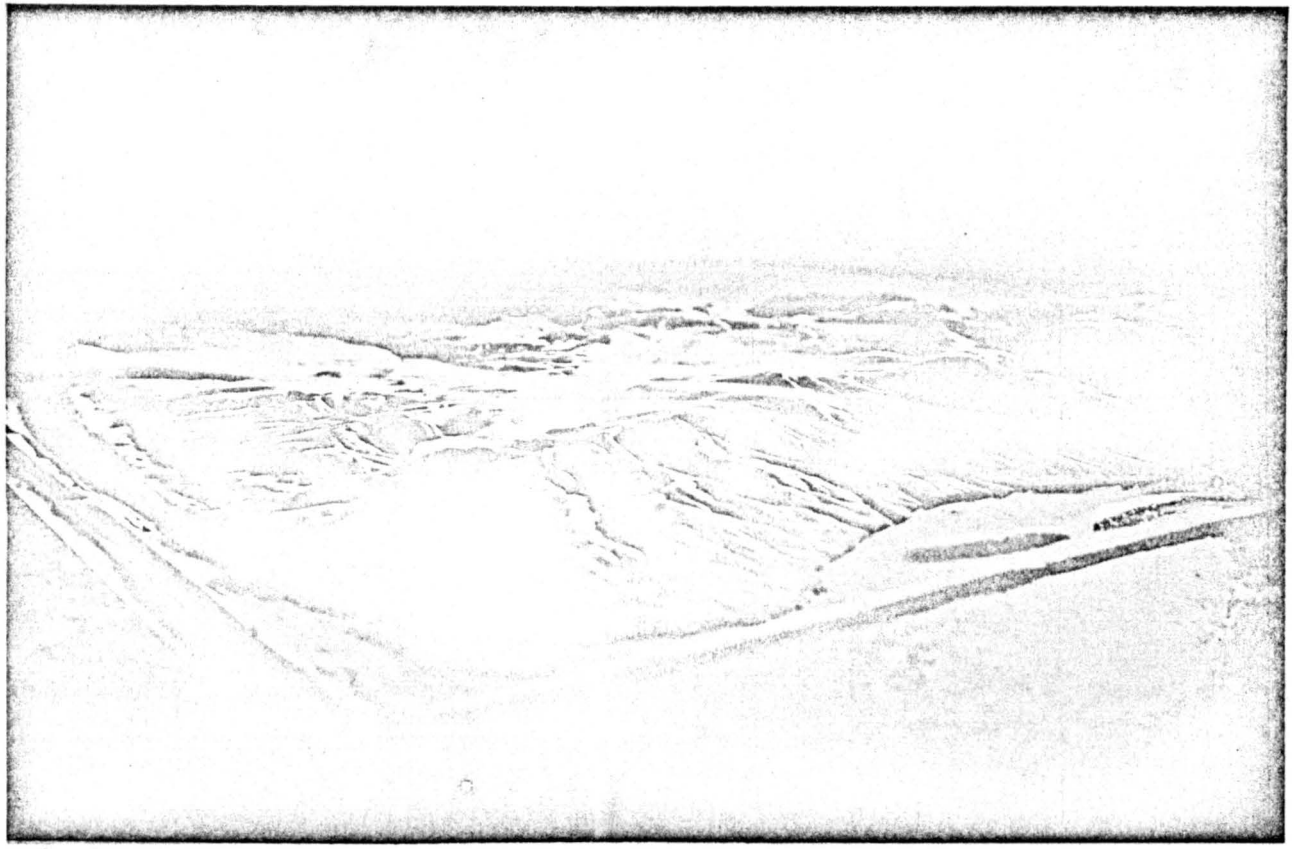

Fig. 26 Smoke flow patterns for $340^0$ ambient flow direction

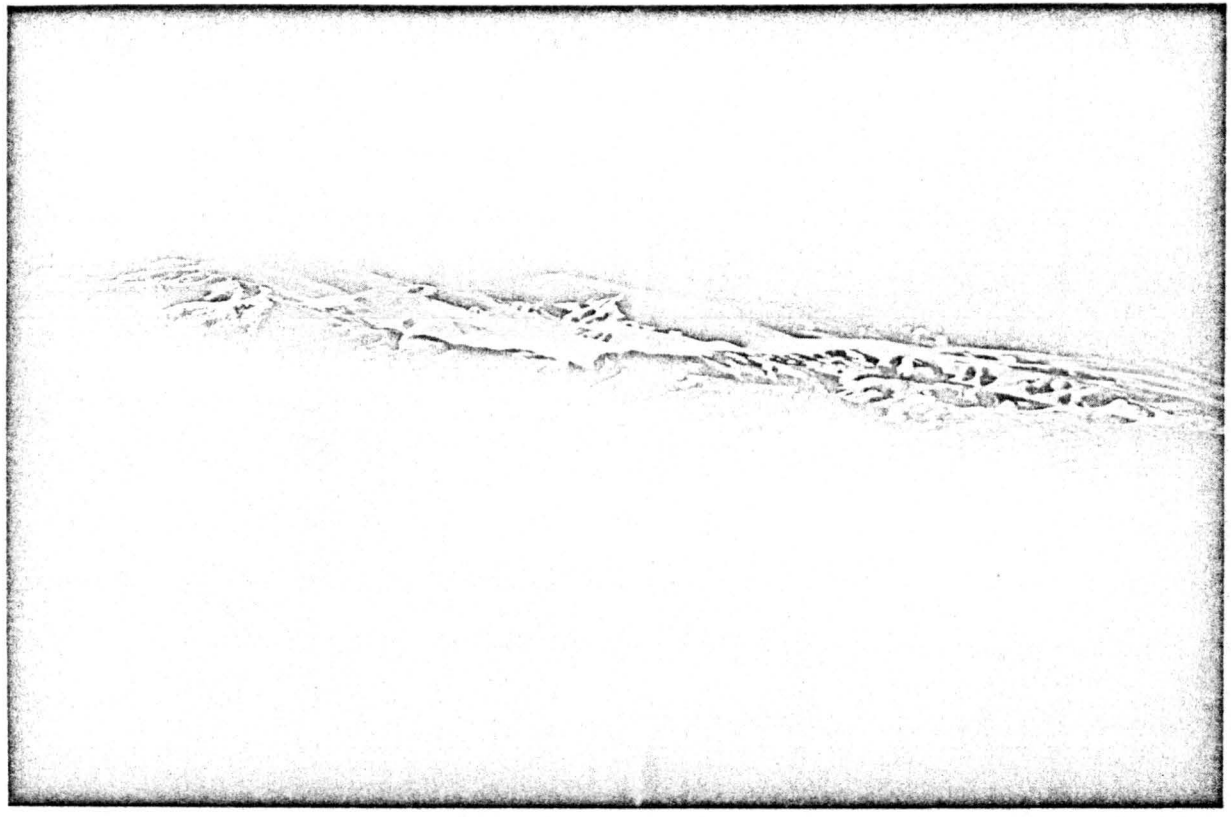

Fig. 27 Smoke flow patterns for $315^0$ ambient flow direction

Fig. 28 Smoke flow patterns for 315° ambient flow direction

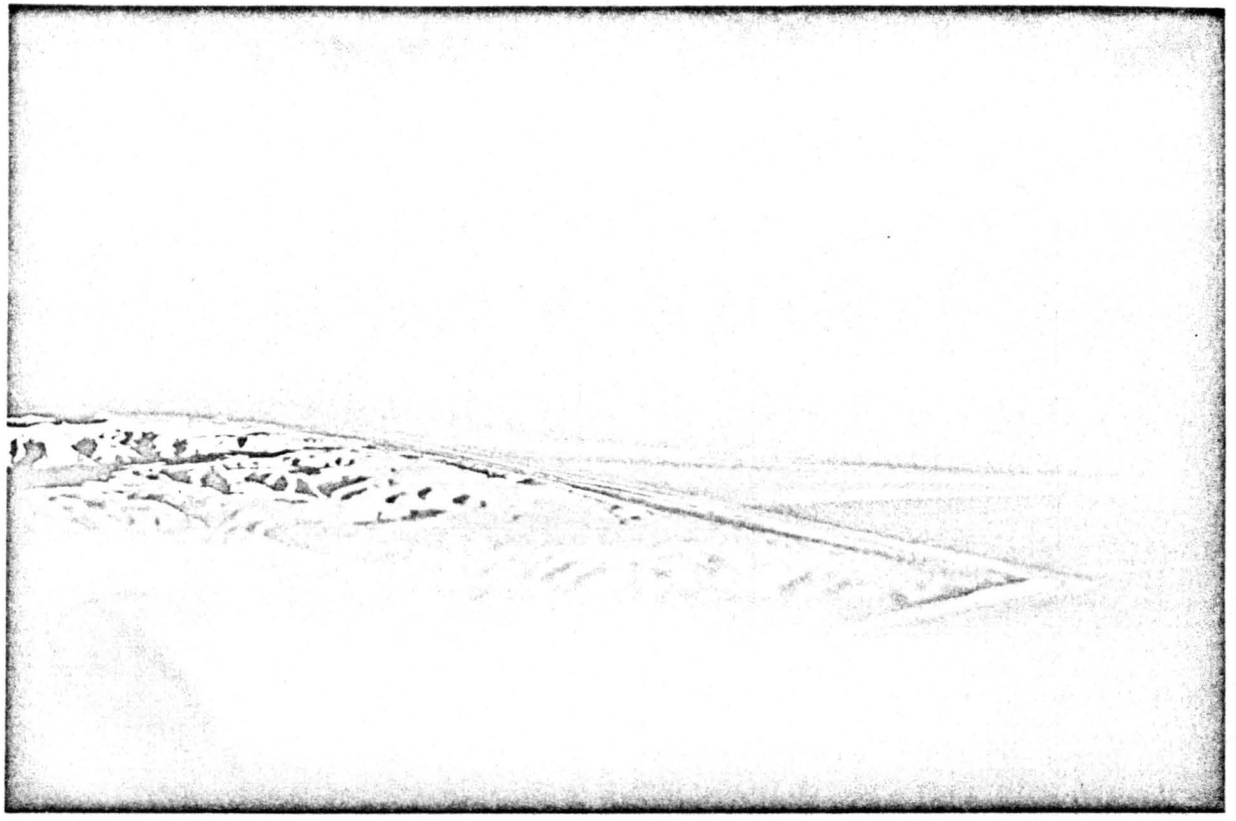

Fig. 29 Smoke flow patterns for $315^0$ ambient flow direction

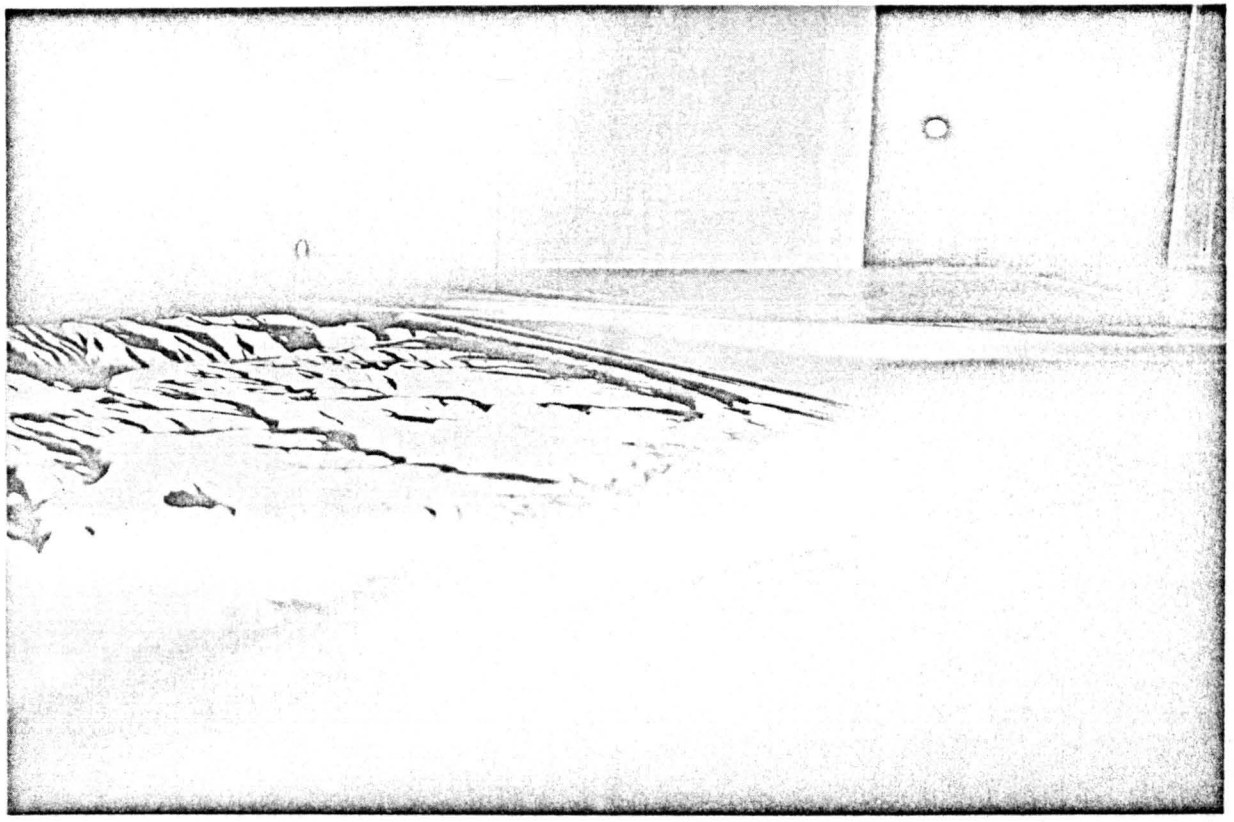

Fig. 30 Smoke flow patterns for $315^0$ ambient flow direction

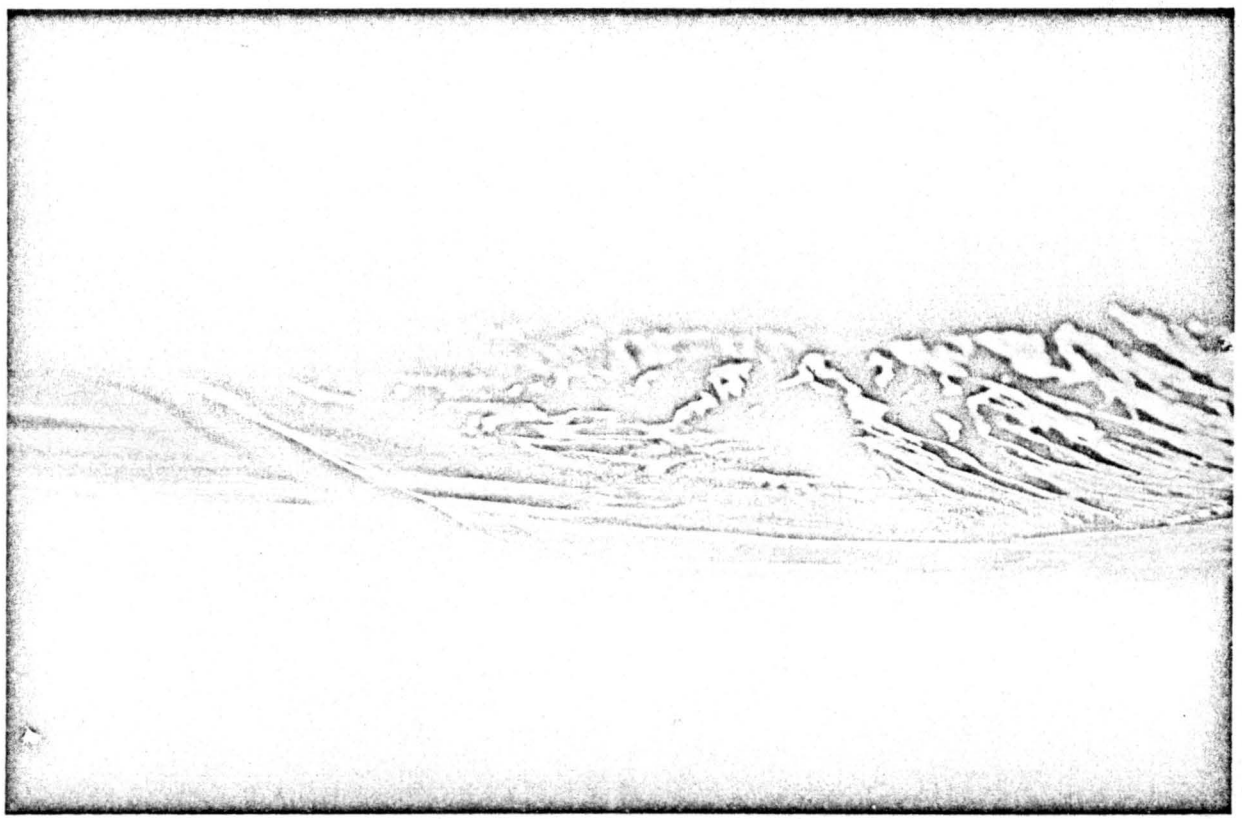

Fig. 31 Smoke flow patterns for $315^0$ ambient flow direction

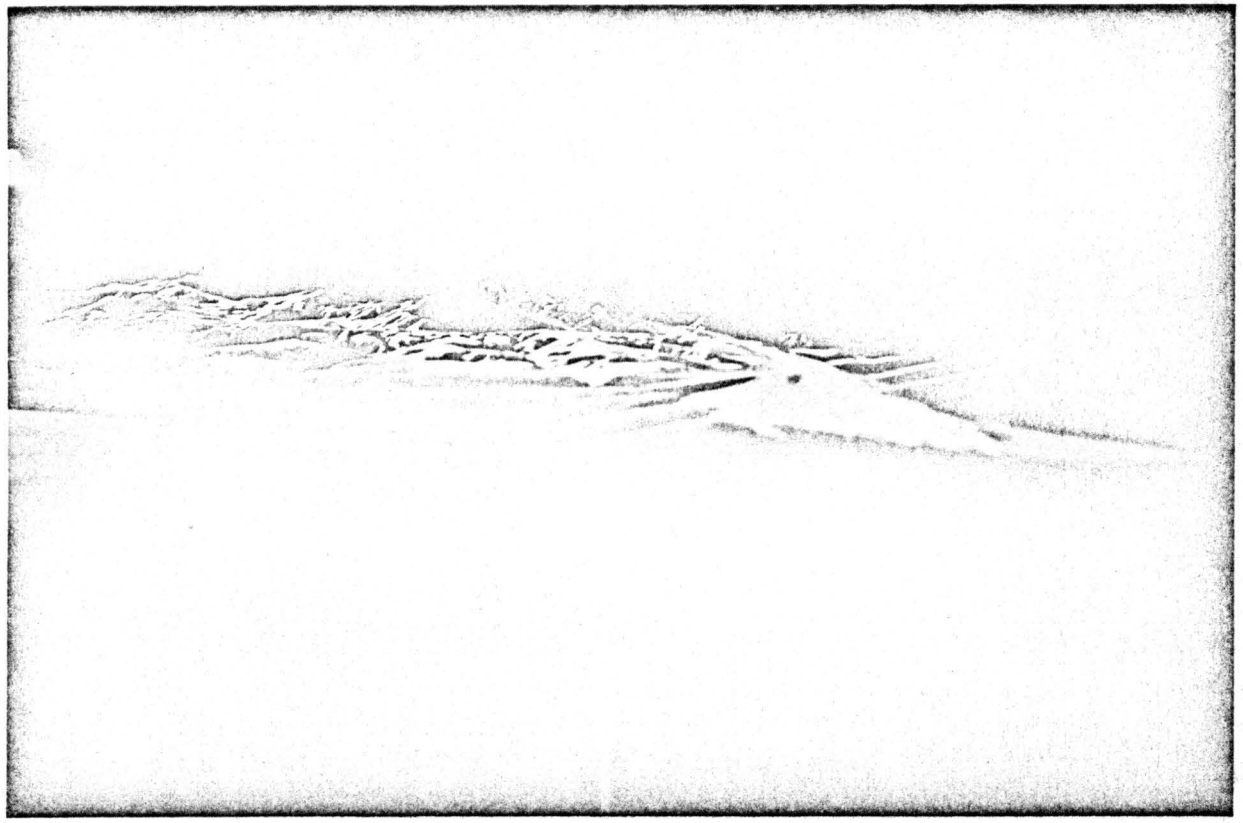

Fig. 32 Smoke flow patterns for $315^0$ ambient flow direction

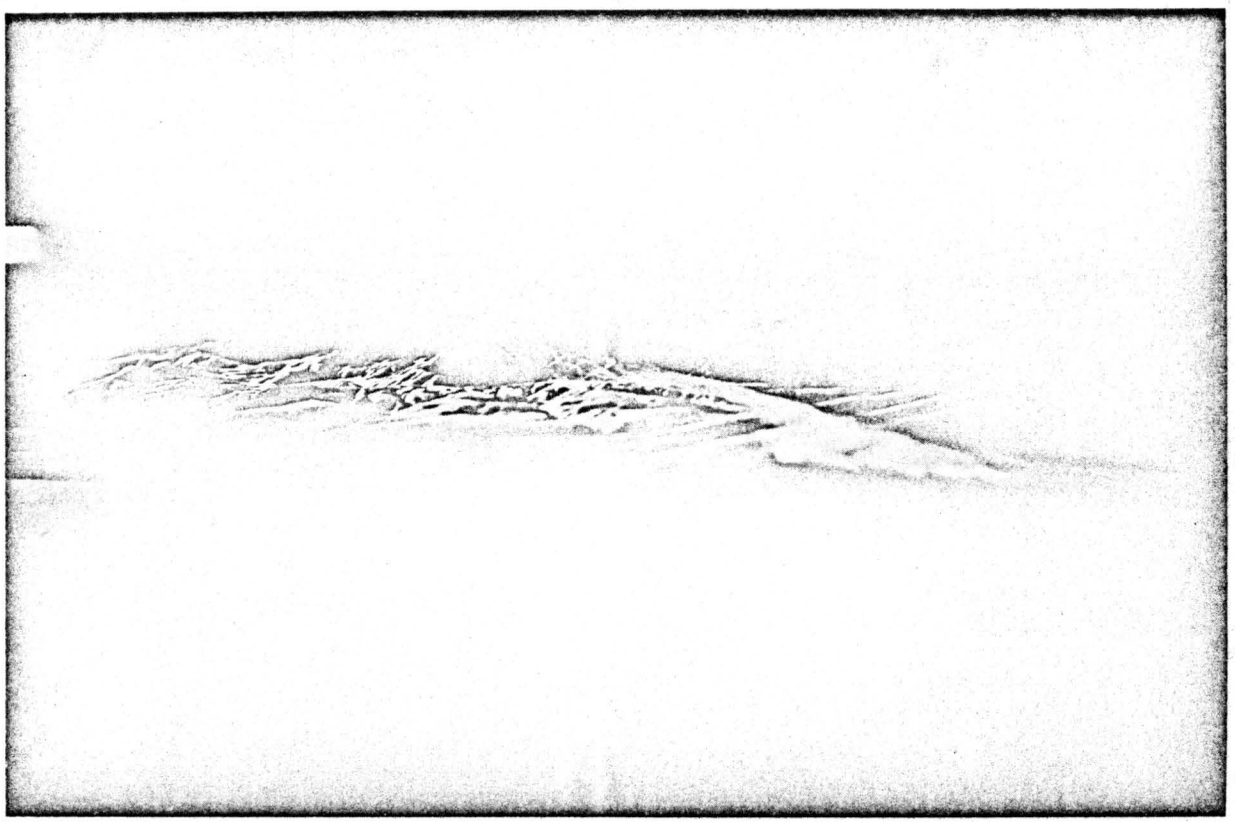

Fig. 33 Smoke flow patterns for $315^0$ ambient flow direction

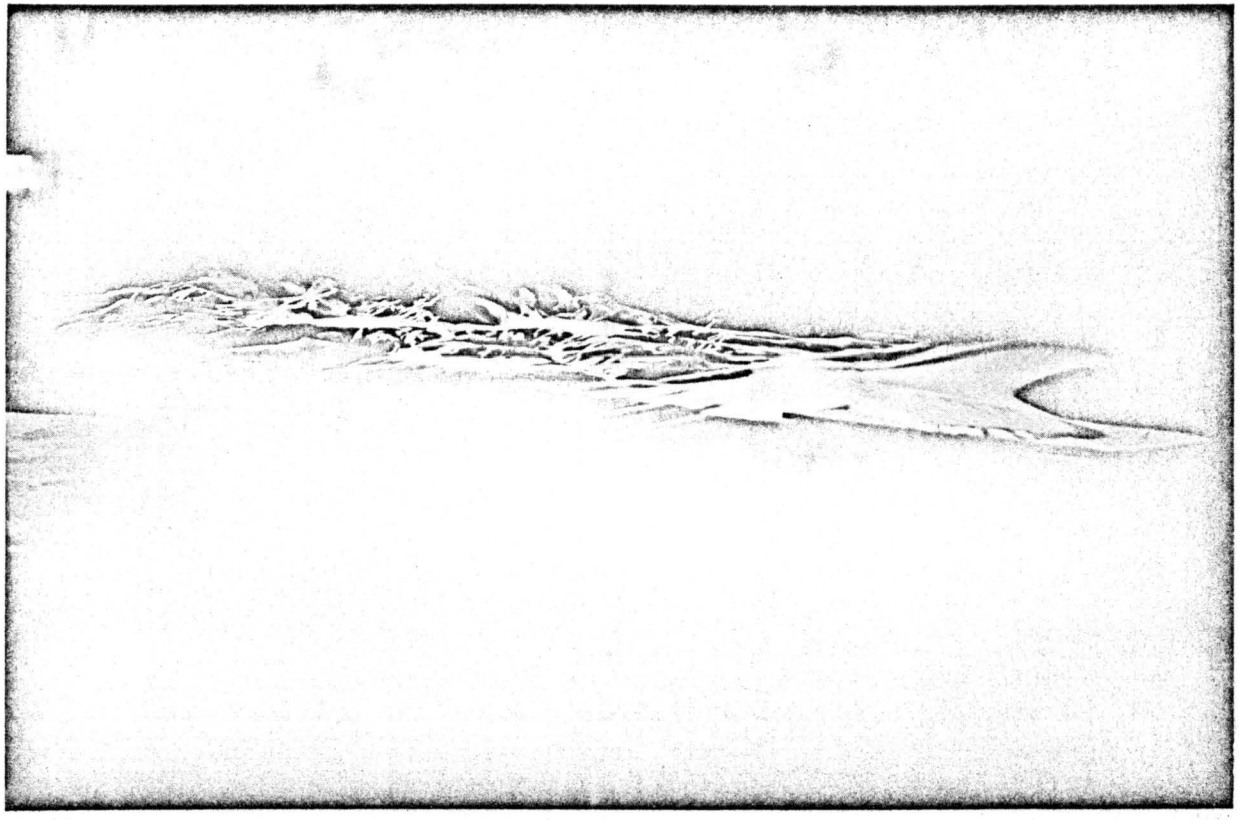

Fig. 34 Smoke flow patterns for $315^0$ ambient flow direction

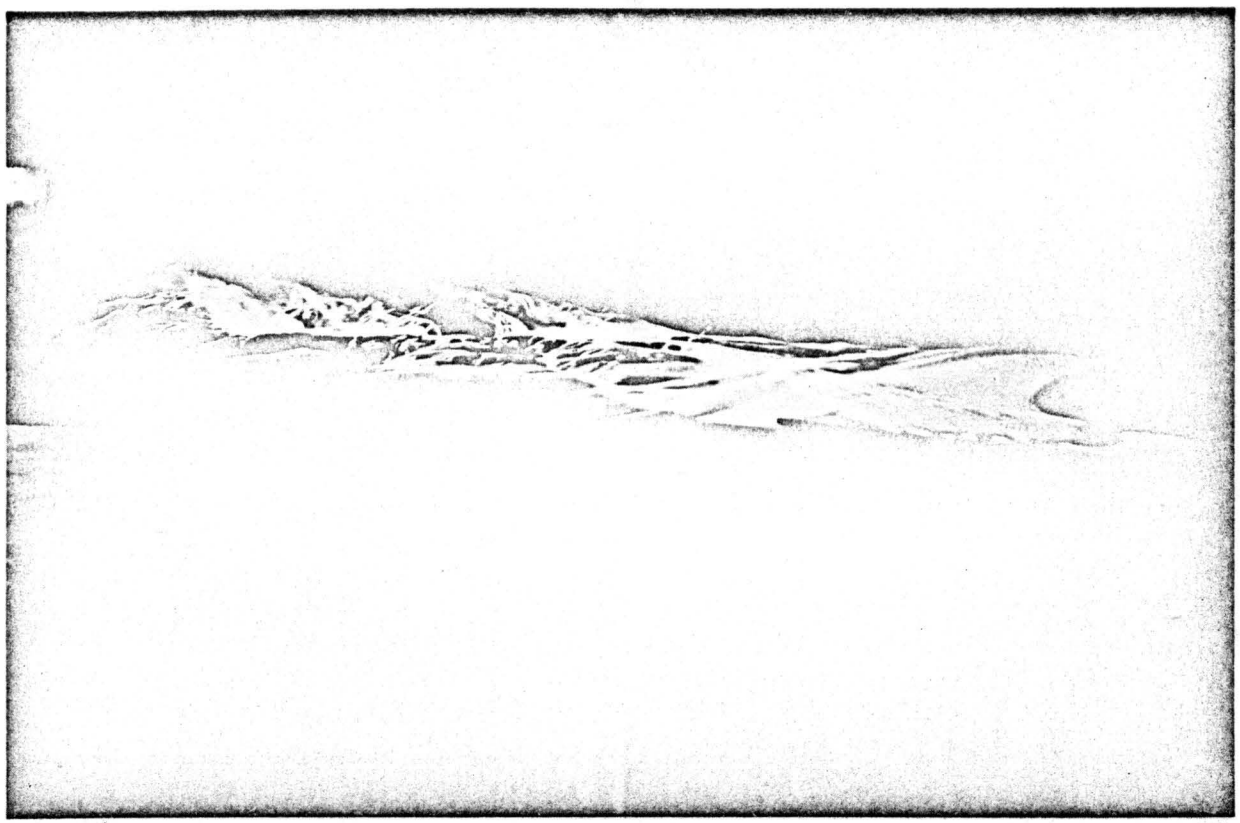

Fig. 35 Smoke flow patterns for $315^0$ ambient flow direction

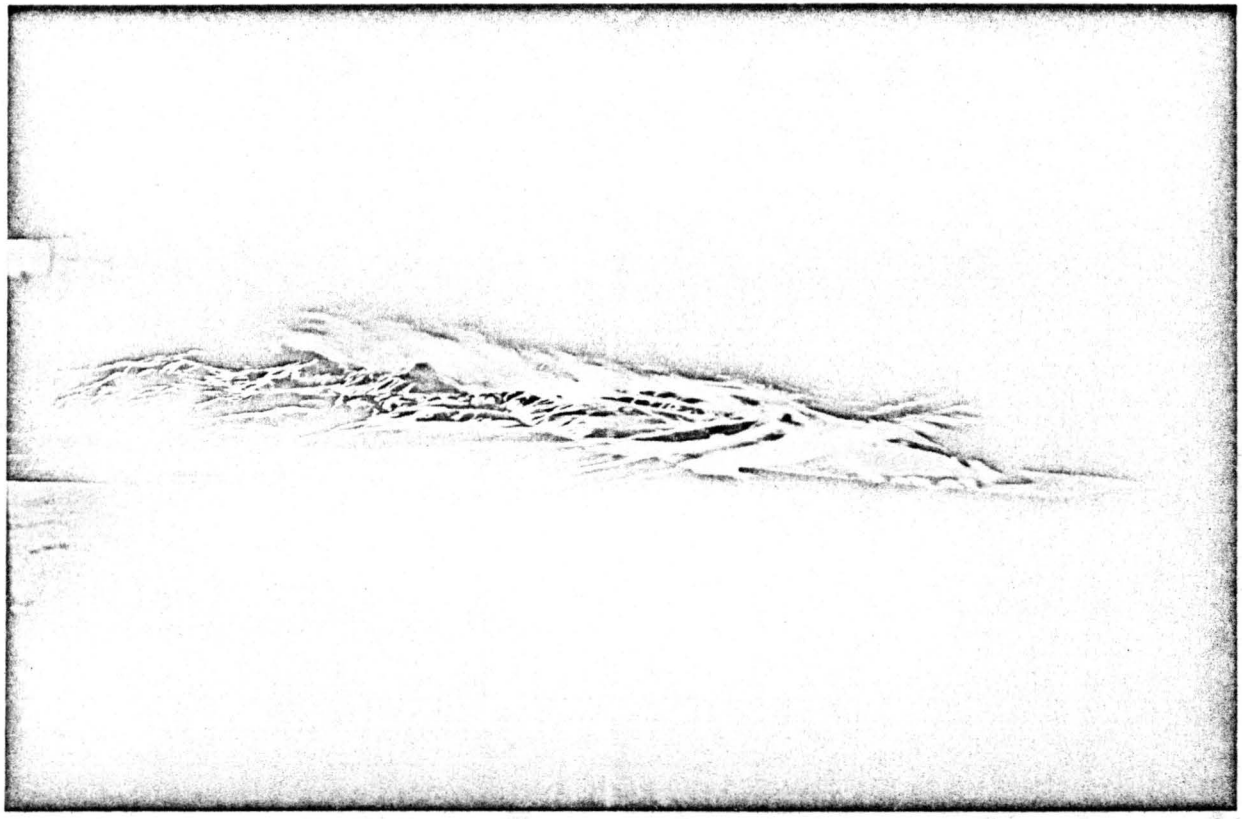

Fig. 36 Smoke flow patterns for $315^0$ ambient flow direction

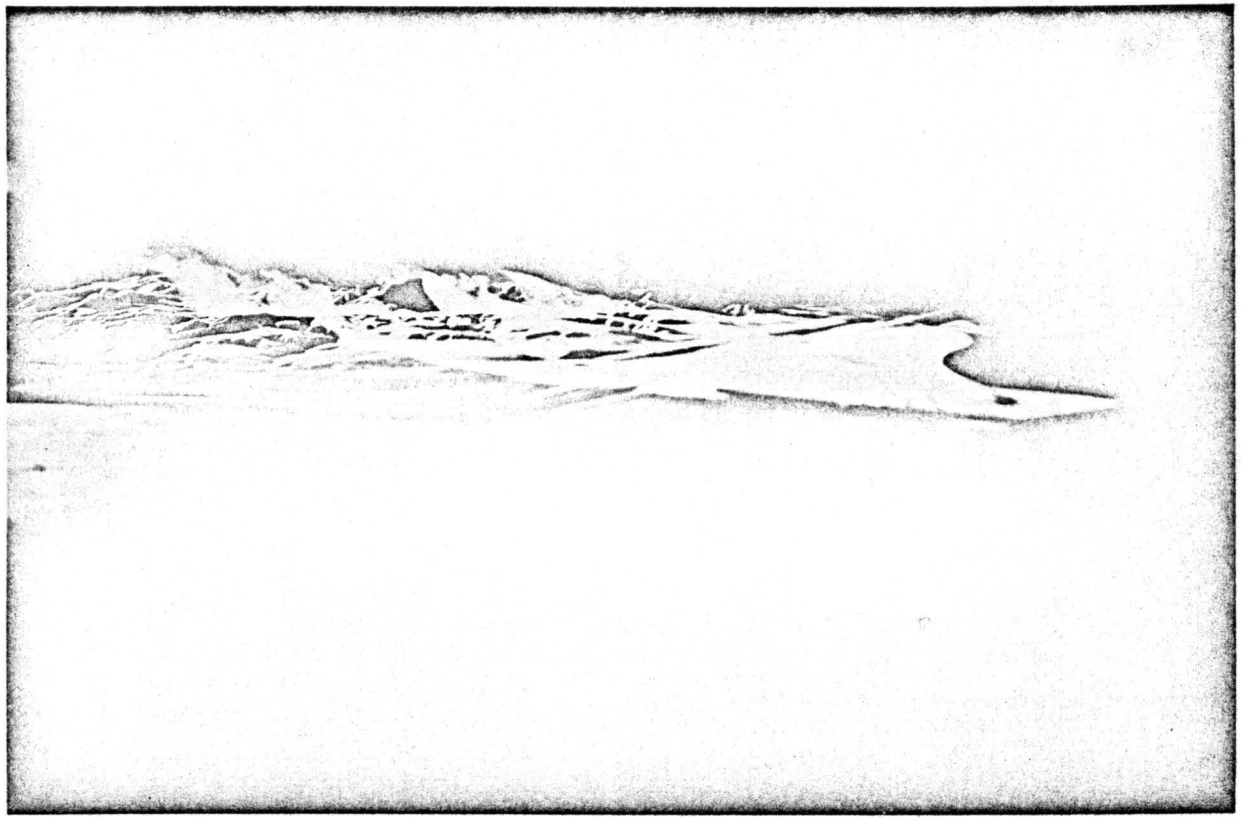

Fig. 37 Smoke flow patterns for 315$^0$ ambient flow direction

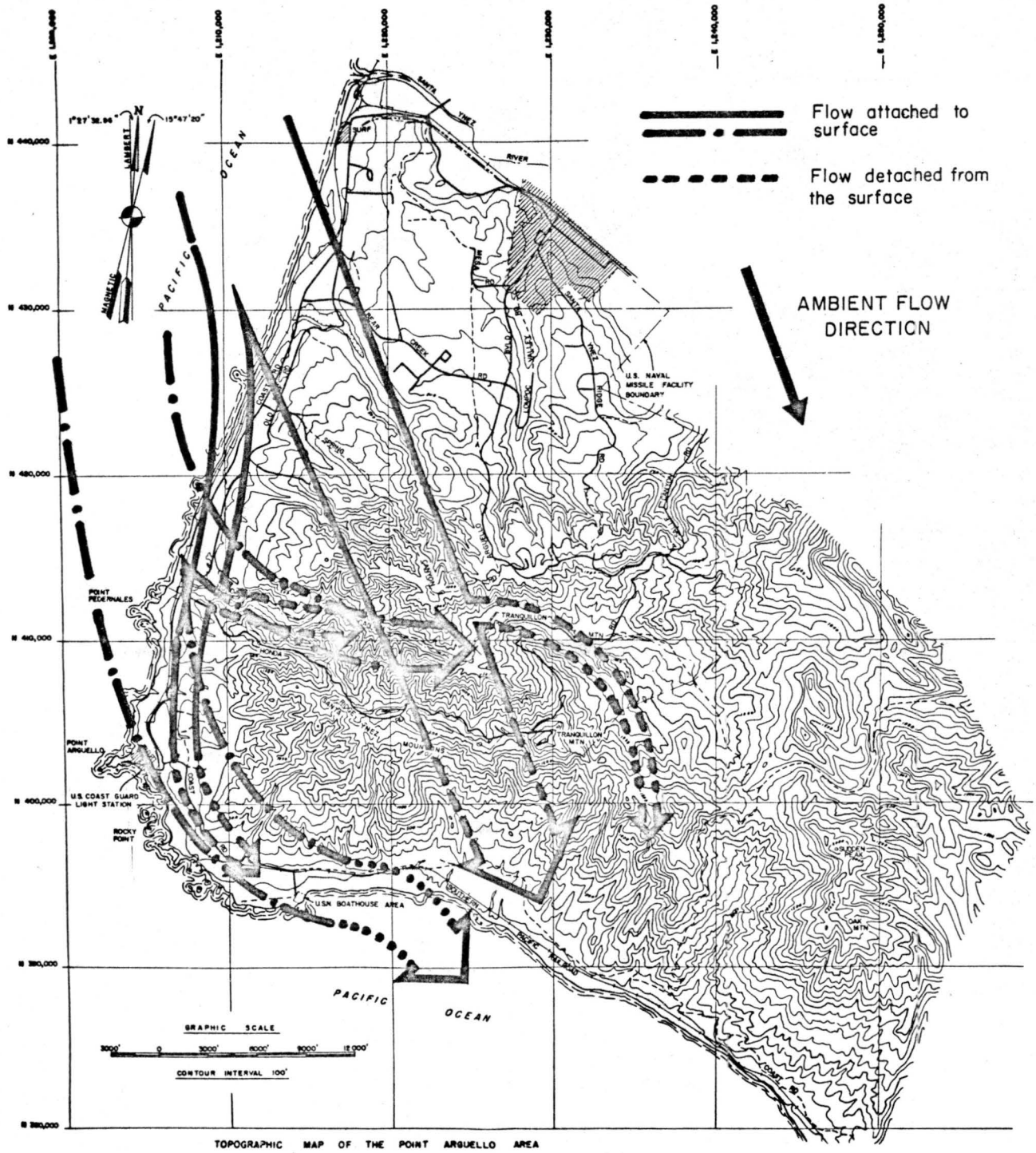


Fig. 38 Mean flow patterns for 340° ambient flow direction with inversion conditions

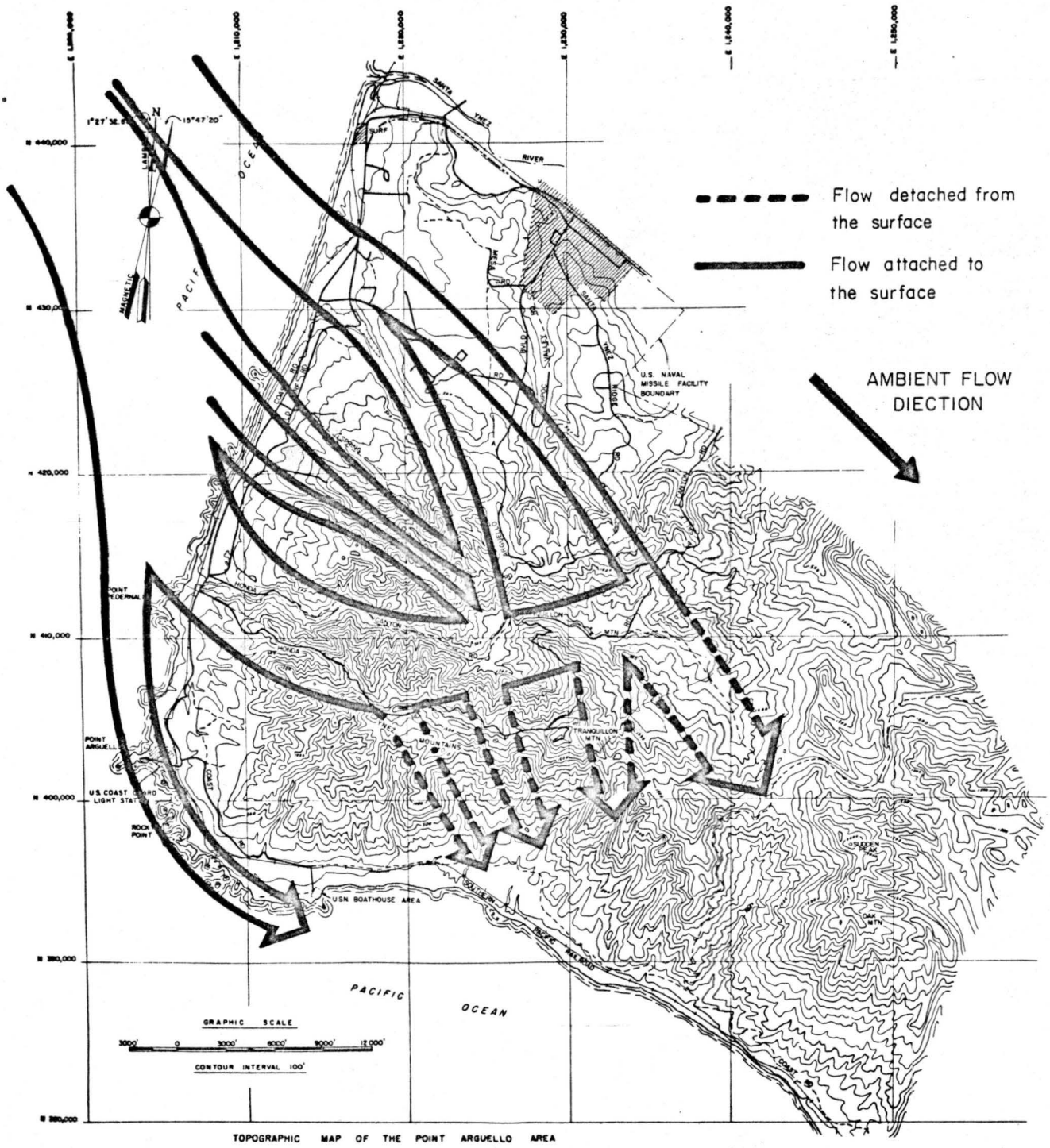


Fig. 39 Mean flow patterns for 315° ambient flow direction with inversion conditions

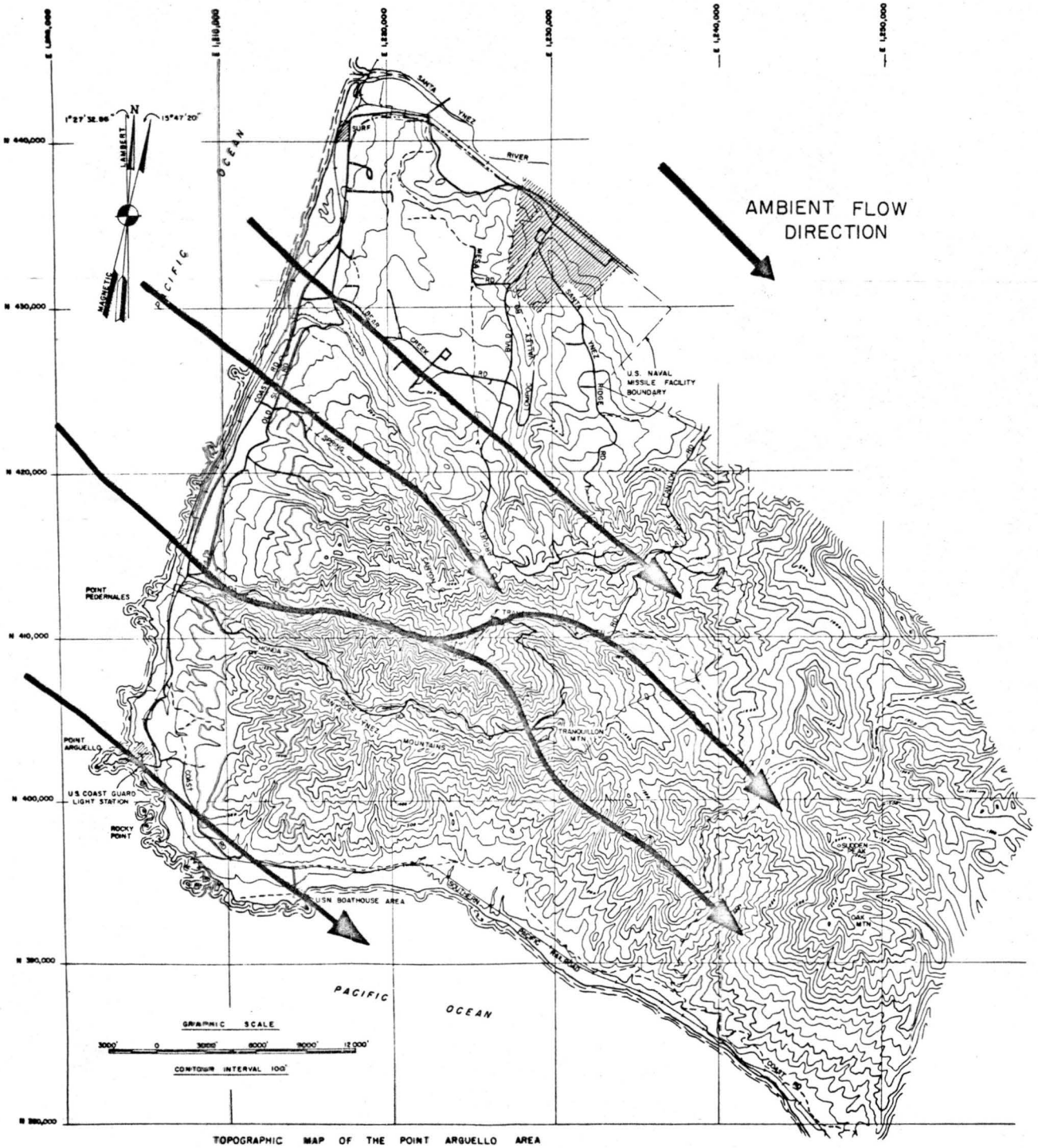


Fig. 40 Mean flow patterns for 315° ambient flow direction with neutral conditions

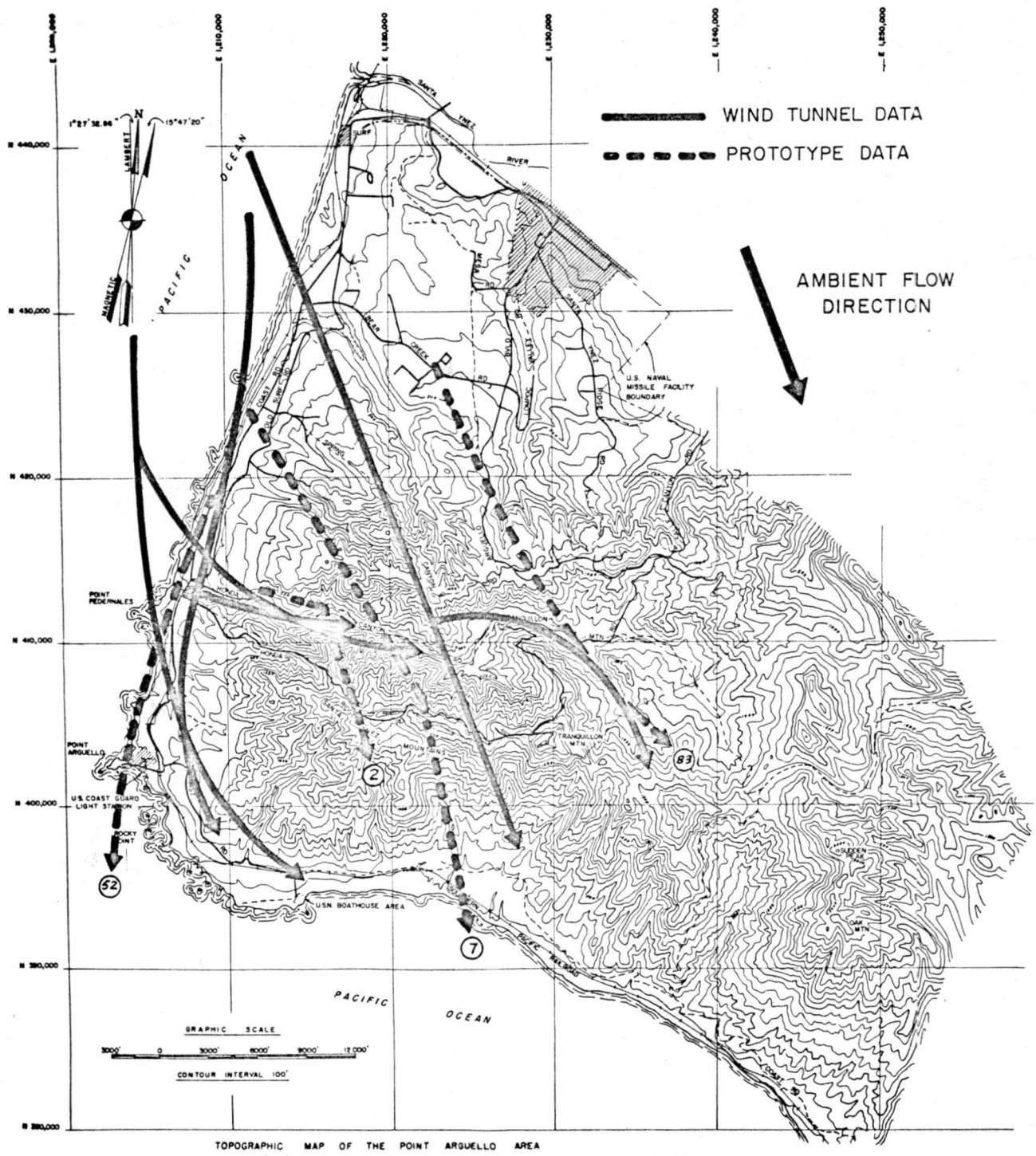


Fig. 41 Comparison of wind tunnel and prototype flow patterns for inversion flow with 340$^0$ ambient wind direction

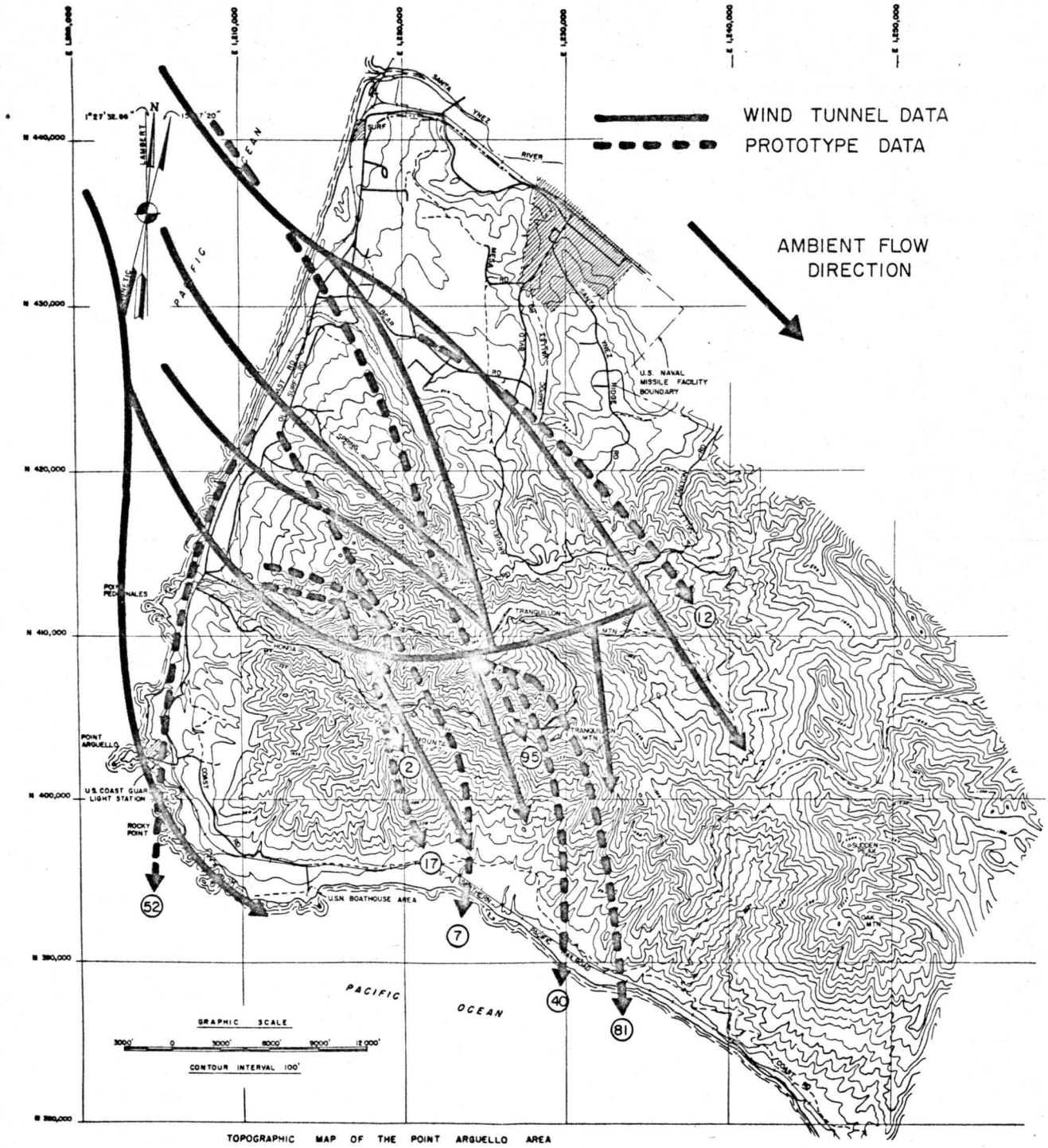


Fig. 42 Comparison of wind tunnel and prototype flow patterns for inversion with 315° ambient wind direction

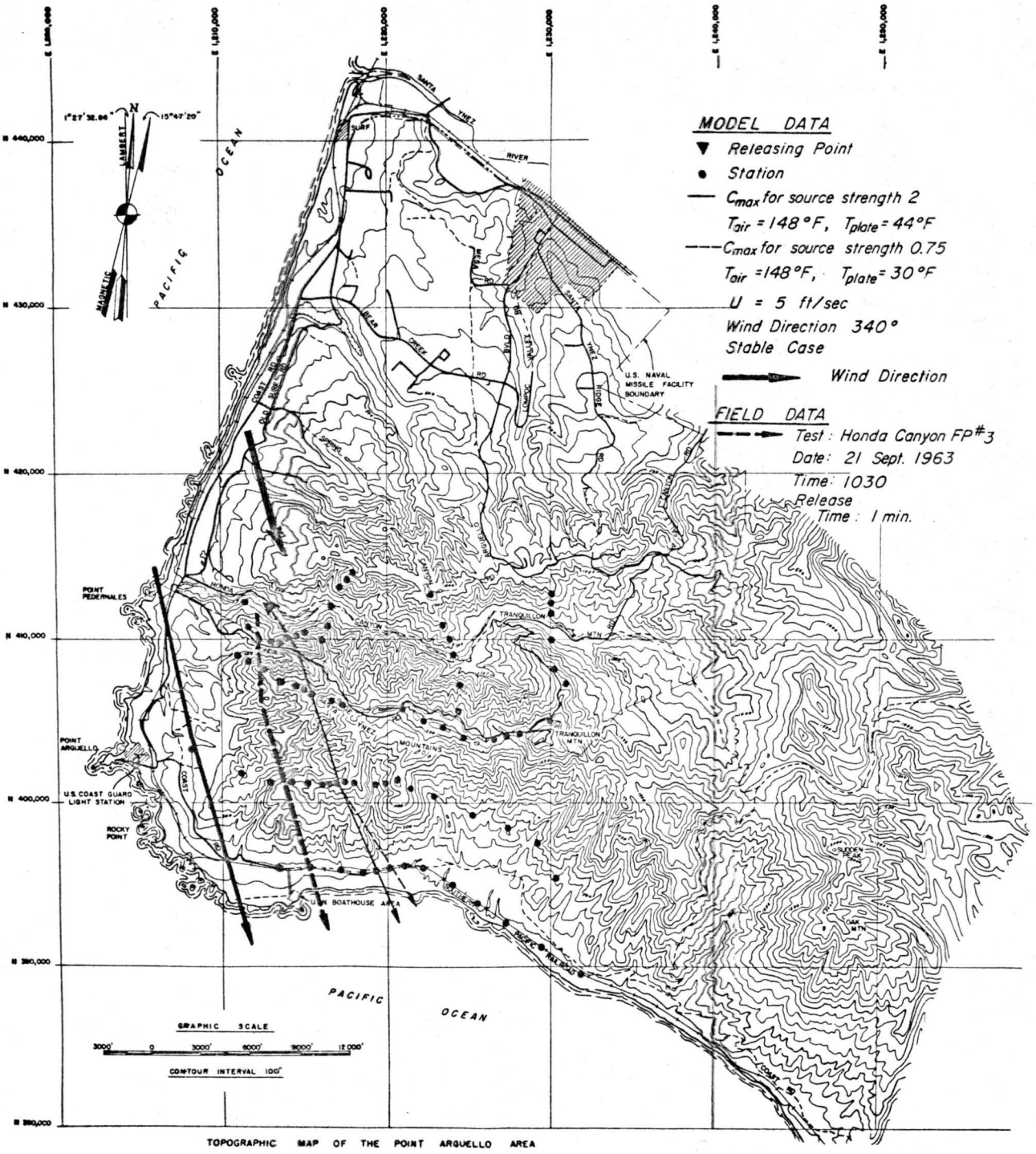


Fig. 43 Comparison of diffusion trajectories for source in Honda Canyon -- 340$^0$ wind

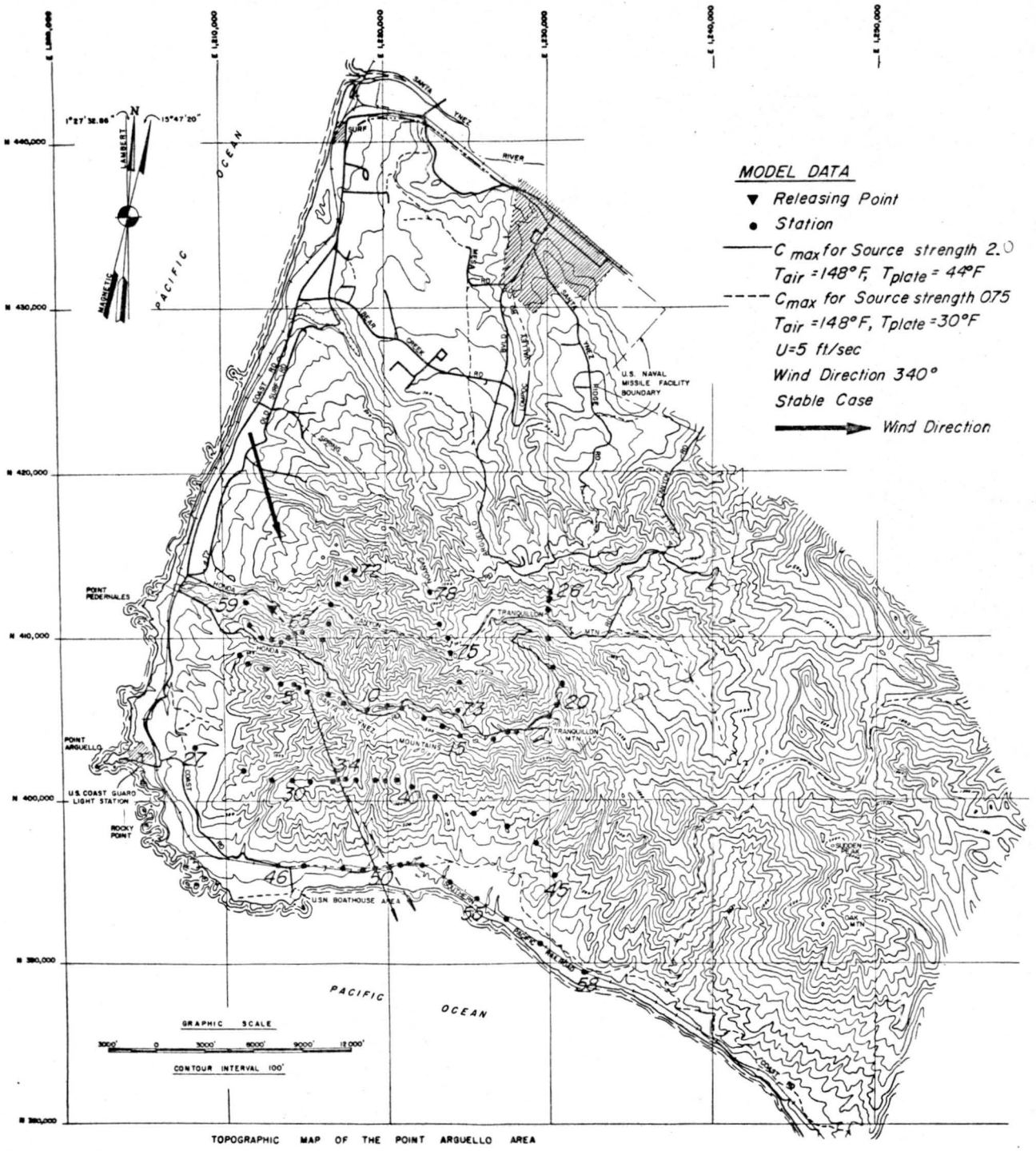


Fig. 44 Distribution of ground-level sampling points

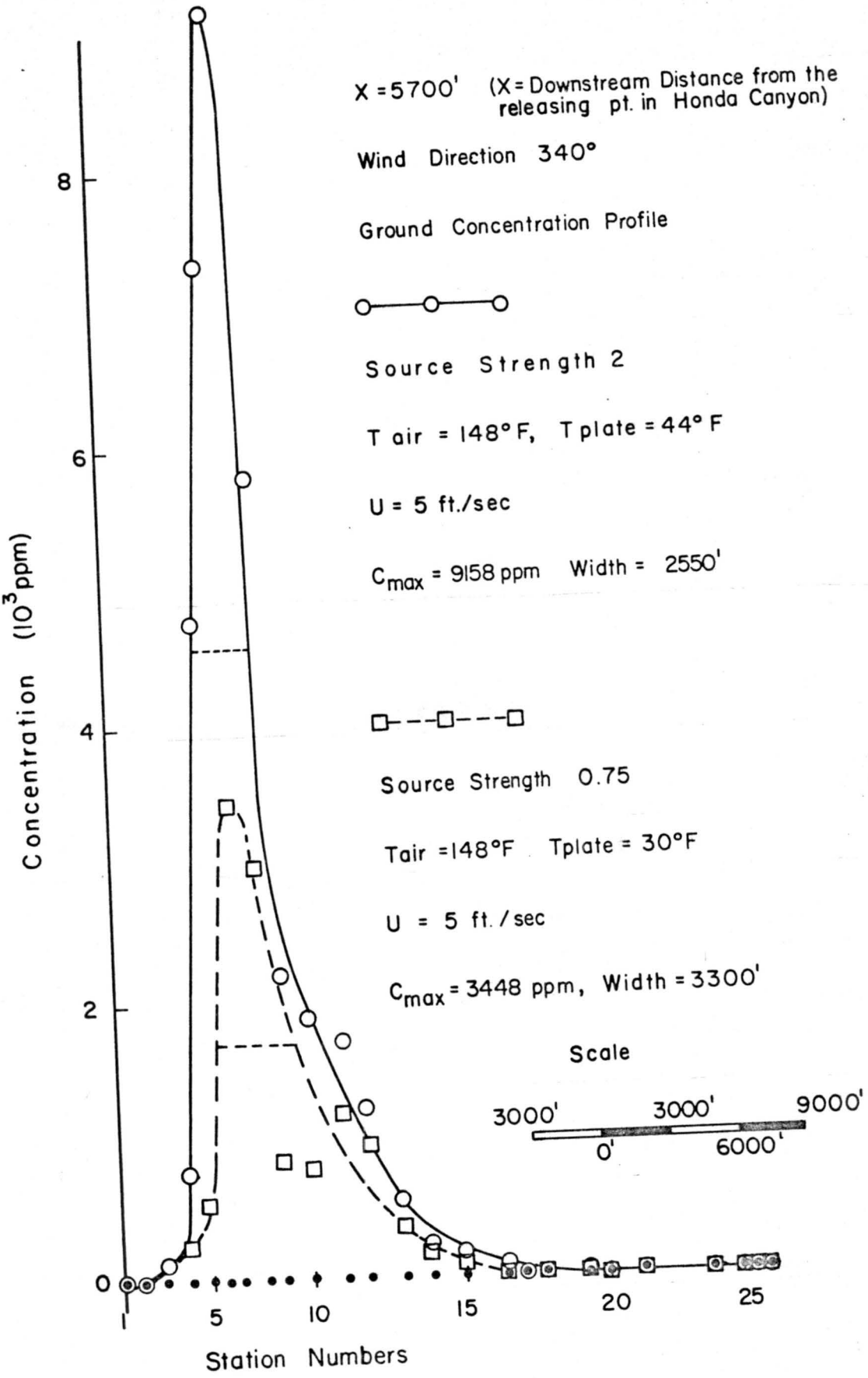


Fig. 45 Ground-level concentration distributions normal to plume axis

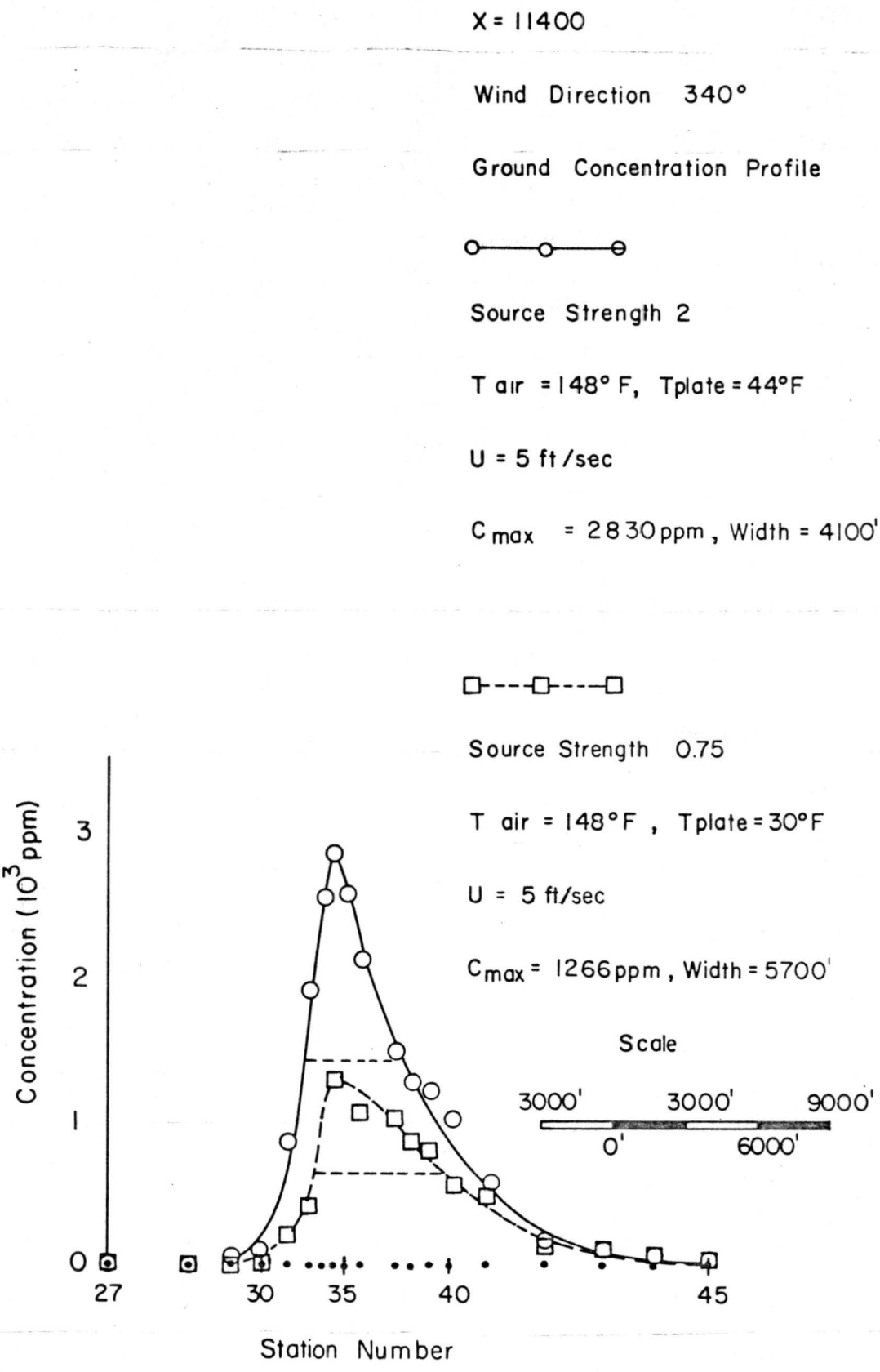


Fig. 46 Ground-level concentration distributions normal to plume axis

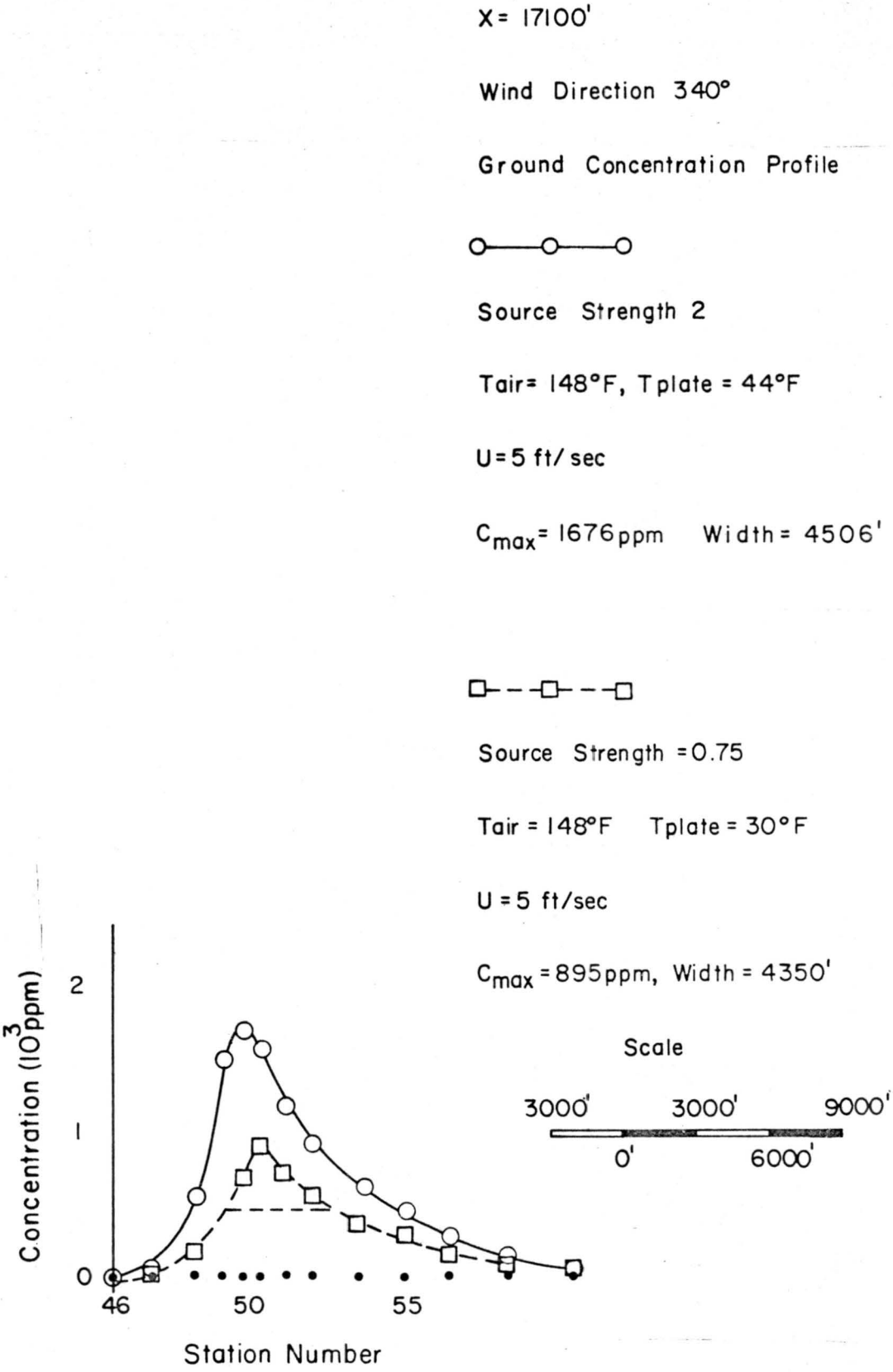


Fig. 47 Ground-level concentration distributions normal to plume axis

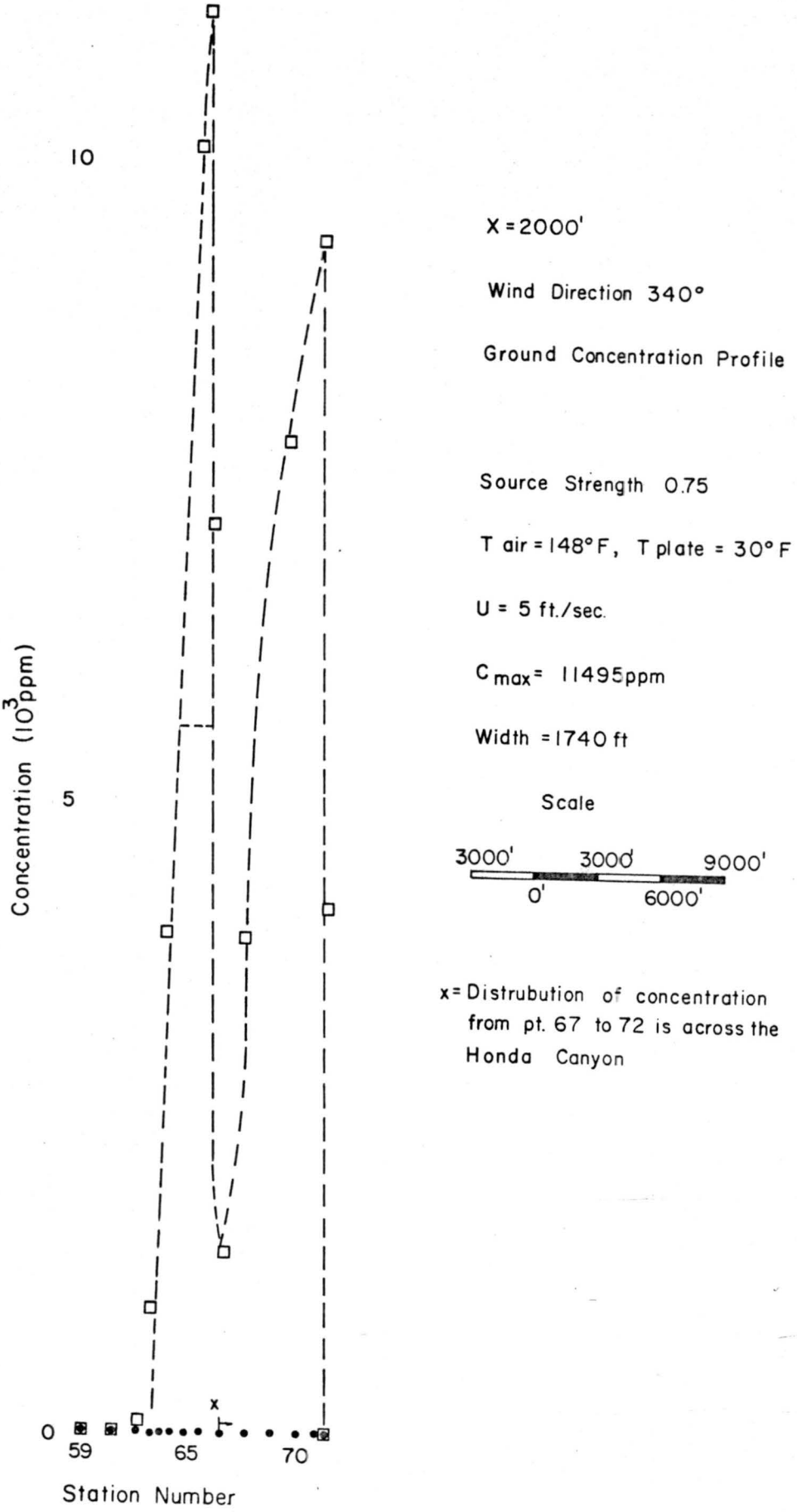


Fig. 48 Ground-level concentration distributions normal to plume axis

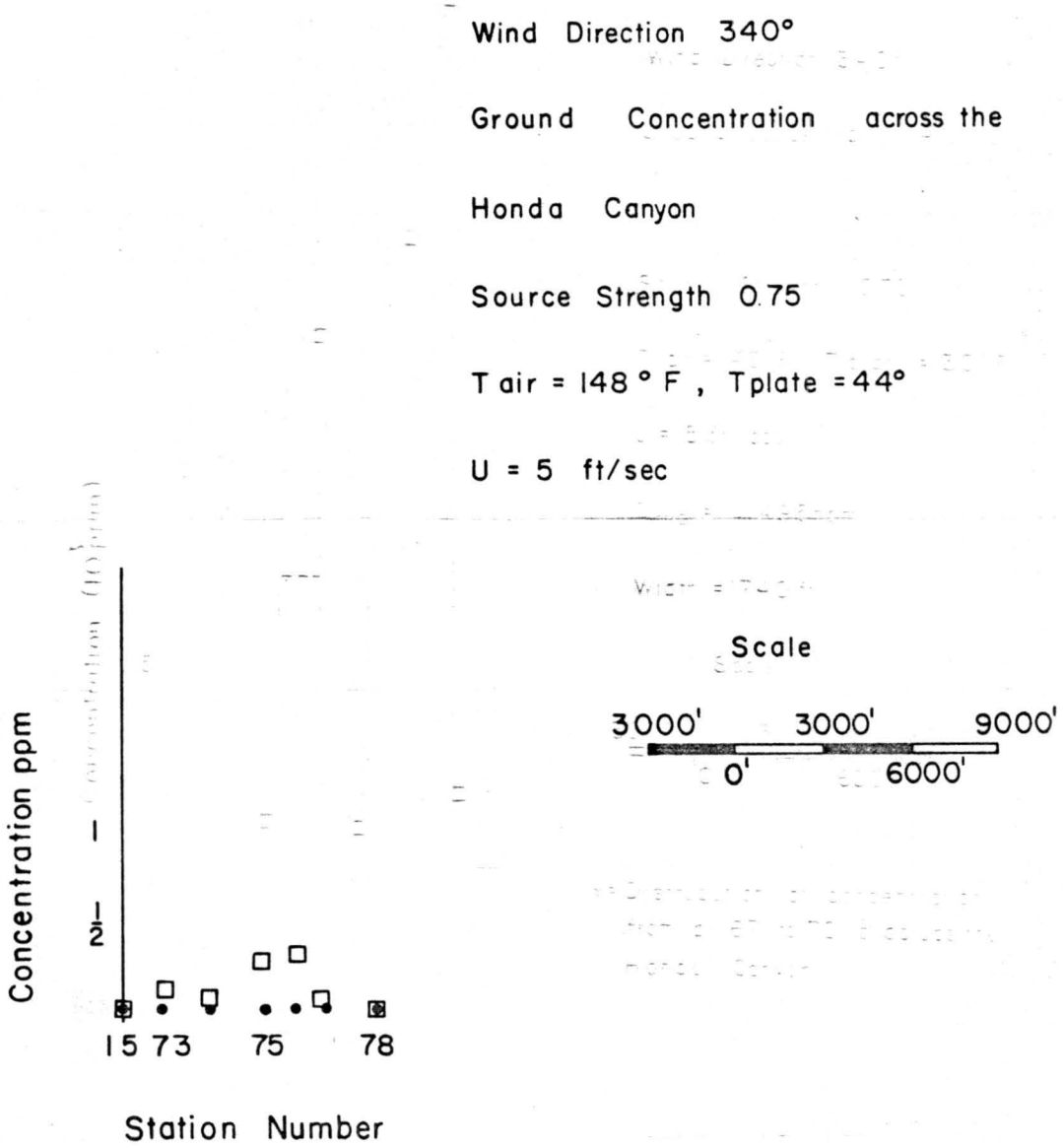


Fig. 49 Ground-level concentration distributions normal to plume axis

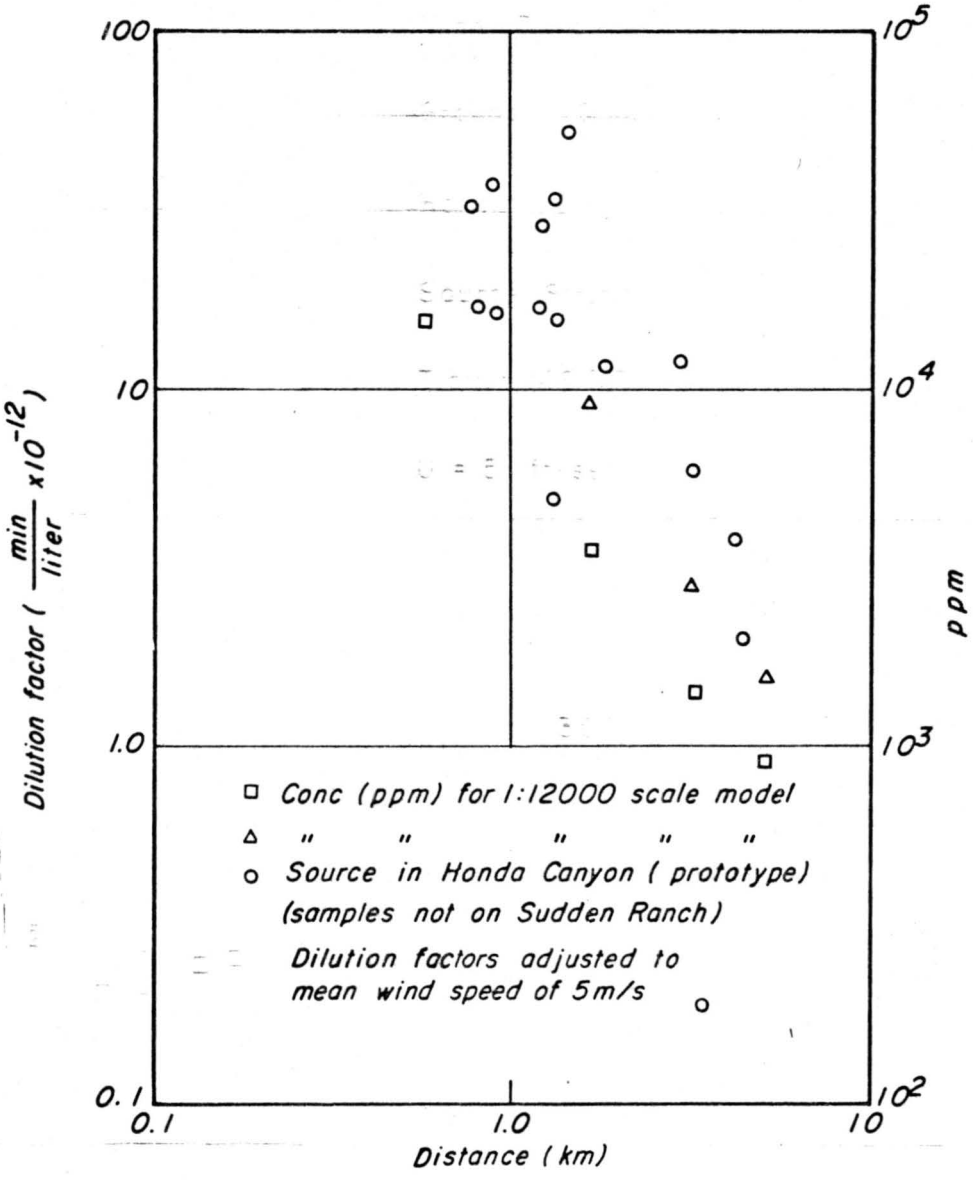


Fig. 50 Downwind variation of dilution and concentration

DOCUMENT CONTROL DATA - R&D

*(Security classification of title, body of abstract and indexing annotation must be entered when the overall report is classified)*

1. ORIGINATING ACTIVITY *(Corporate author)*
Fluid Mechanics Program, College of Engineering
Colorado State University
Fort Collins, Colorado

2a. REPORT SECURITY CLASSIFICATION
Unclassified

2b. GROUP
Unclassified

3. REPORT TITLE
SIMULATION OF WIND FIELDS OVER POINT ARGUELLO, CALIFORNIA BY WIND-TUNNEL FLOW OVER A TOPOGRAPHIC MODEL.

4. DESCRIPTIVE NOTES *(Type of report and inclusive dates)*
Final Technical Report

5. AUTHOR(S) *(Last name, first name, initial)*
Cermak, J. E., and Jon Peterka

| 6. REPORT DATE | 7a. TOTAL NO. OF PAGES | 7b. NO. OF REFS |
|---|---|---|
| November 1966 | 83 | 10 |

8a. CONTRACT OR GRANT NO.
N 123(61756)34361 A (PMR)

b. PROJECT NO.
2236

c.

d.

9a. ORIGINATOR'S REPORT NUMBER(S)
CER65JEC-JAP64

9b. OTHER REPORT NO(S) *(Any other numbers that may be assigned this report)*

10. AVAILABILITY/LIMITATION NOTICES
Distribution of this document is unlimited

11. SUPPLEMENTARY NOTES

12. SPONSORING MILITARY ACTIVITY
U.S. Navy Purchasing Office
929 South Broadway
Los Angeles, California 90055

13. ABSTRACT

Stably stratified flow over a 1:12,000 scale model of the U.S. Naval Missile Facility at Point Arguello, California was studied in the Army Meteorological wind tunnel of the Fluid Dynamics and Diffusion Laboratory at Colorado State University. Mean temperature, mean velocity and mean concentration distribution obtained for the laboratory flow were compared with available field data collected at the site. These comparisons revealed that the geometrical, dynamic and thermal similarity were sufficiently achieved to give similar mean flow patterns, temperature distributions and concentration decay rates for diffusing tracers.

The data revealed that a laminar laboratory flow may be used to simulate a turbulent field flow under conditions of stable thermal stratification and complex terrain. In such flow conditions diffusion is dominated by convective dispersion.

| 14. KEY WORDS | LINK A | | LINK B | | LINK C | |
|---|---|---|---|---|---|---|
| | ROLE | WT | ROLE | WT | ROLE | WT |
| Simulation | | | | | | |
| Atmospheric modeling | | | | | | |
| Stratified flow | | | | | | |
| Diffusion | | | | | | |
| Wind-tunnel laboratory | | | | | | |
| Laminar flow | | | | | | |
| Fluid mechanics | | | | | | |
| Micrometeorology | | | | | | |
| Mesometeorology | | | | | | |

INSTRUCTIONS

1. ORIGINATING ACTIVITY: Enter the name and address of the contractor, subcontractor, grantee, Department of Defense activity or other organization *(corporate author)* issuing the report.

2*a*. REPORT SECURITY CLASSIFICATION: Enter the overall security classification of the report. Indicate whether "Restricted Data" is included. Marking is to be in accordance with appropriate security regulations.

2*b*. GROUP: Automatic downgrading is specified in DoD Directive 5200.10 and Armed Forces Industrial Manual. Enter the group number. Also, when applicable, show that optional markings have been used for Group 3 and Group 4 as authorized.

3. REPORT TITLE: Enter the complete report title in all capital letters. Titles in all cases should be unclassified. If a meaningful title cannot be selected without classification, show title classification in all capitals in parenthesis immediately following the title.

4. DESCRIPTIVE NOTES: If appropriate, enter the type of report, e.g., interim, progress, summary, annual, or final. Give the inclusive dates when a specific reporting period is covered.

5. AUTHOR(S): Enter the name(s) of author(s) as shown on or in the report. Enter last name, first name, middle initial. If military, show rank and branch of service. The name of the principal author is an absolute minimum requirement.

6. REPORT DATE: Enter the date of the report as day, month, year; or month, year. If more than one date appears on the report, use date of publication.

7*a*. TOTAL NUMBER OF PAGES: The total page count should follow normal pagination procedures, i.e., enter the number of pages containing information.

7*b*. NUMBER OF REFERENCES: Enter the total number of references cited in the report.

8*a*. CONTRACT OR GRANT NUMBER: If appropriate, enter the applicable number of the contract or grant under which the report was written.

8*b*, 8*c*, & 8*d*. PROJECT NUMBER: Enter the appropriate military department identification, such as project number, subproject number, system numbers, task number, etc.

9*a*. ORIGINATOR'S REPORT NUMBER(S): Enter the official report number by which the document will be identified and controlled by the originating activity. This number must be unique to this report.

9*b*. OTHER REPORT NUMBER(S): If the report has been assigned any other report numbers *(either by the originator or by the sponsor)*, also enter this number(s).

10. AVAILABILITY/LIMITATION NOTICES: Enter any limitations on further dissemination of the report, other than those imposed by security classification, using standard statements such as:

(1) "Qualified requesters may obtain copies of this report from DDC."

(2) "Foreign announcement and dissemination of this report by DDC is not authorized."

(3) "U. S. Government agencies may obtain copies of this report directly from DDC. Other qualified DDC users shall request through _____."

(4) "U. S. military agencies may obtain copies of this report directly from DDC. Other qualified users shall request through _____."

(5) "All distribution of this report is controlled. Qualified DDC users shall request through _____."

If the report has been furnished to the Office of Technical Services, Department of Commerce, for sale to the public, indicate this fact and enter the price, if known.

11. SUPPLEMENTARY NOTES: Use for additional explanatory notes.

12. SPONSORING MILITARY ACTIVITY: Enter the name of the departmental project office or laboratory sponsoring *(paying for)* the research and development. Include address.

13. ABSTRACT: Enter an abstract giving a brief and factual summary of the document indicative of the report, even though it may also appear elsewhere in the body of the technical report. If additional space is required, a continuation sheet shall be attached.

It is highly desirable that the abstract of classified reports be unclassified. Each paragraph of the abstract shall end with an indication of the military security classification of the information in the paragraph, represented as *(TS)*, *(S)*, *(C)*, or *(U)*.

There is no limitation on the length of the abstract. However, the suggested length is from 150 to 225 words.

14. KEY WORDS: Key words are technically meaningful terms or short phrases that characterize a report and may be used as index entries for cataloging the report. Key words must be selected so that no security classification is required. Identifiers, such as equipment model designation, trade name, military project code name, geographic location, may be used as key words but will be followed by an indication of technical context. The assignment of links, rules, and weights is optional.